iScience

CellPress
OPEN ACCESS

Article

CASK loss of function differentially regulates neuronal maturation and synaptic function in human induced cortical excitatory neurons

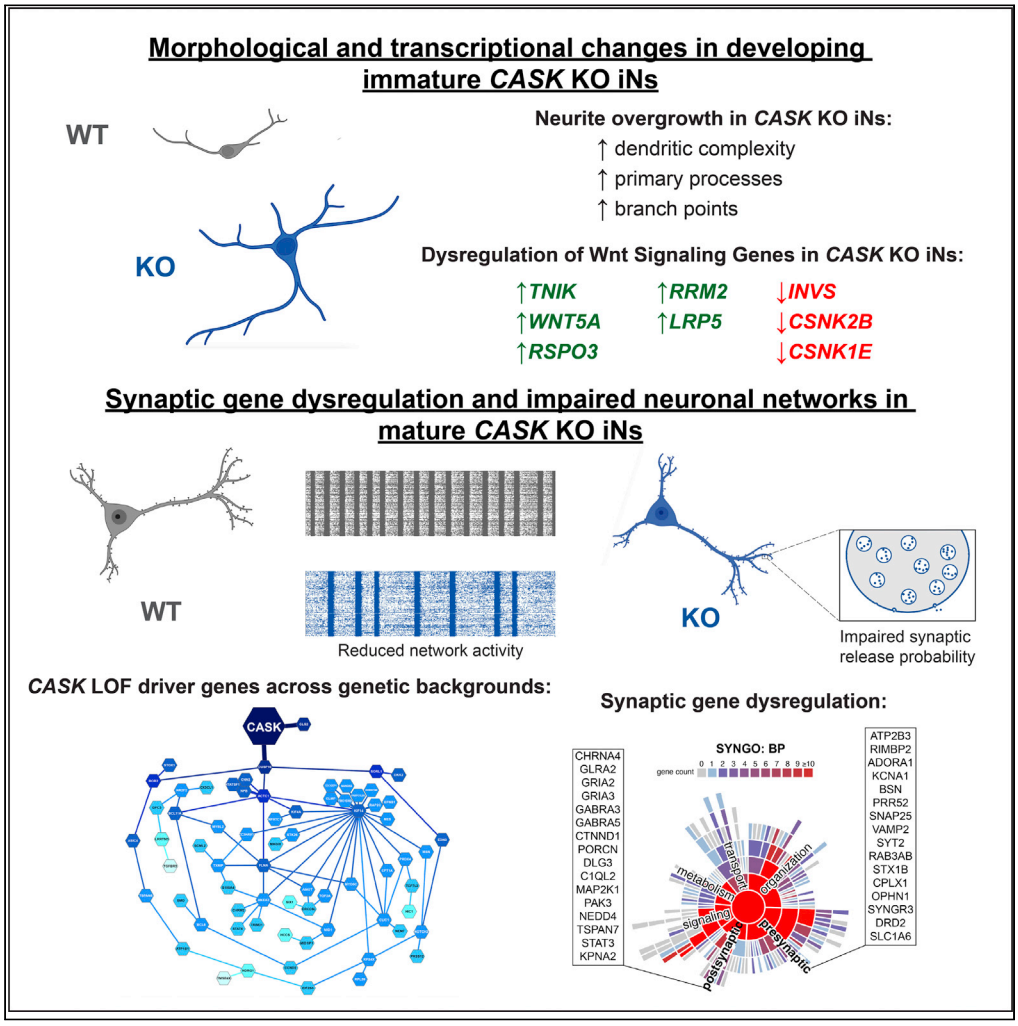

Danny McSweeney, Rafael Gabriel, Kang Jin, Zhiping P. Pang, Bruce Aronow, ChangHui Pak

cpak@umass.edu

Highlights

Human-induced excitatory neuronal model of *CASK* deficiency

CASK LOF mutations increase neuronal complexity in developing excitatory neurons

CASK LOF causes synaptic impairment in mature excitatory neurons

CASK mutations regulate a core set of genes across genetic backgrounds

McSweeney et al., iScience 25, 105187
October 21, 2022
https://doi.org/10.1016/j.isci.2022.105187

iScience

CellPress
OPEN ACCESS

Article

CASK loss of function differentially regulates neuronal maturation and synaptic function in human induced cortical excitatory neurons

Danny McSweeney,[1,2] Rafael Gabriel,[2] Kang Jin,[3] Zhiping P. Pang,[4] Bruce Aronow,[3] and ChangHui Pak[2,5,*]

SUMMARY

Loss-of-function (LOF) mutations in *CASK* cause severe developmental phenotypes, including microcephaly with pontine and cerebellar hypoplasia, X-linked intellectual disability, and autism. Unraveling the pathological mechanisms of *CASK*-related disorders has been challenging owing to limited human cellular models to study the dynamic roles of this molecule during neuronal maturation and synapse development. Here, we investigate cell-autonomous functions of *CASK* in cortical excitatory induced neurons (iNs) generated from *CASK* knockout (KO) isogenic human embryonic stem cells (hESCs) using gene expression, morphometrics, and electrophysiology. While immature *CASK* KO iNs show robust neuronal outgrowth, mature *CASK* KO iNs display severe defects in synaptic transmission and synchronized network activity without compromising neuronal morphology and synapse numbers. In the developing human cortical excitatory neurons, CASK functions to promote both structural integrity and establishment of cortical excitatory neuronal networks. These results lay the foundation for future studies identifying suppressors of such phenotypes relevant to human patients.

INTRODUCTION

Defining the molecular and cellular mechanisms underlying neurodevelopmental disorders (NDDs) is crucial for developing novel therapeutics and treatments for patients with these devastating conditions. Advances in genome-wide association studies (GWAS) and identification of genetic variants associated with NDDs, even those with heterogeneous polygenic origin, have expanded new fertile grounds for disease mechanistic studies linking genetic variants to human phenotypes. *CASK*-related disorders present such a case. Located on chromosome Xp11.4, *CASK* encodes a multi-domain scaffolding molecule named calcium/calmodulin-dependent serine protein kinase (Hata et al., 1996; Hsueh, 2009). To date, multiple genetic variants of *CASK* have been identified in the human patient population, including microcephaly with pontine and cerebellar hypoplasia (MICPCH), X-linked intellectual disability (XLID), FG syndrome, developmental delays, and autism spectrum disorders (ASDs) (Froyen et al., 2007; Najm et al., 2008; Piluso et al., 2003; de Vries et al., 2002). Despite the rich human genetic findings, our understanding of how *CASK* loss-of-function (LOF) mutations impact neurodevelopment and function in the developing human brain is lacking. This challenge stems from the limited access to patient fetal brain tissue and the pleiotropic and multi-faceted nature of *CASK* function in the nervous system.

CASK is ubiquitously expressed in the brain with the ability to bind to and work with multiple proteins in various cellular compartments over the course of development. In the developing rodent neurons, Cask shuttles into the nucleus to regulate gene expression of N-methyl-D-aspartate receptor (NMDAR) subunit 2b (*NR2b*) and Reelin (*Reln*) by binding to T-box transcription factor Tbr1 and CINAP (CASK-interacting nucleosome assembly protein) (Hsueh et al., 2000; Wang et al., 2004a, 2004b). During synapse development, Cask's prominent role at the presynapse is as a scaffold, interacting with N-type calcium channels, adapter proteins (Veli, Mint, Liprin-alpha), and cell adhesion molecules (Neurexin-1), thereby maintaining the molecular architecture for efficient neurotransmitter release (Butz et al., 1998; Hata et al., 1996; LaConte et al., 2016; Mukherjee et al., 2008; Olsen et al., 2005; Spangler et al., 2013). At the postsynapse, Cask interacts with cell adhesion molecule Syndecan-2 to regulate the stability/maintenance of dendritic spines by triggering downstream signaling events mediated by the NF1-PKA-Ena/VASP pathway (Chao et al., 2008;

[1]Graduate Program in Molecular and Cellular Biology, UMass Amherst, Amherst, MA 01003, USA

[2]Department of Biochemistry and Molecular Biology, UMass Amherst, Amherst, MA 01003, USA

[3]Departments of Biomedical Informatics, Pediatrics, University of Cincinnati, Cincinnati Children's Hospital Medical Center, Cincinnati, OH 45229, USA

[4]Child Health Institute of New Jersey and Department of Neuroscience and Cell Biology, Robert Wood Johnson Medical School, Rutgers University, New Brunswick, NJ 08901, USA

[5]Lead contact

*Correspondence: cpak@umass.edu

https://doi.org/10.1016/j.isci.2022.105187

Lin et al., 2007). Cask also functions as a bridge between the plasma membrane and the F-actin cytoskeleton via binding to protein 4.1 (Chao et al., 2008). Furthermore, in *Drosophila*, CASK physically binds to CaMKII and regulates the phosphorylation status of CaMKII, suggesting that CASK acts as an activity sensor controlling a major signaling hub at the synapse upon neuronal activity (Hodge et al., 2006; Lu et al., 2003).

Despite these illuminating studies linking CASK to cortical development and synapse maturation, mammalian and human cellular models of *CASK* LOF have been elusive. Although the diversity of CASK function has been demonstrated through biochemical studies, many of these interactions have been performed with limited domains and lack the cellular context details, making it difficult to pinpoint exactly its normal function during brain and synapse development. Moreover, while invertebrate studies strongly support the role of CASK in synaptic transmission at neuromuscular junctions (Chen and Featherstone, 2011; Zordan et al., 2005), *Cask* KO in mice leads to perinatal lethality (Atasoy et al., 2007). In surviving animals, subtle changes in synaptic transmission are apparent (increased miniature excitatory postsynaptic currents and decreased miniature inhibitory postsynaptic currents) with normal ultrastructure of synapses, suggesting that the function of this molecule can be different and more complicated in mammals (Atasoy et al., 2007). More recently, novel genetic mouse models using an X-inactivation scheme reported defects in excitatory/inhibitory (E/I) balance and decreased *NR2b* mRNA levels in heterozygous *Cask* KO mosaic females (Mori et al., 2019). This defect was primarily rescued by restoring *NR2b*, suggesting a postsynaptic mechanism (Mori et al., 2019). Additional studies in mice reported not only synaptic but also metabolic roles of *Cask* during neurodevelopment (Patel et al., 2020; Srivastava et al., 2016). In comparison, bulk RNA sequencing (RNA-seq) of human induced pluripotent stem cell (iPSC)-neurons derived from two *CASK* mutation carriers (a male with autism and a female with intellectual disability) revealed the downregulation of a set of presynaptic genes and CASK interactors along with some deficits in inhibitory presynaptic puncta size in one patient background (Becker et al., 2020). However, owing to heterogeneity in patient genetic background, sex, and nature of *CASK* mutations, patient iPSC-derived neuronal studies require multiple cell lines and proper controls. Therefore, there is a critical need to use isogenic lines of *CASK* LOF to provide a clean genetic background from which one can assess the effects of *CASK* LOF without the influence of complex genetic backgrounds.

Here, we describe an approach using CRISPR/Cas9 gene editing in human embryonic stem cells (hESCs) to generate two independent *CASK* KO isogenic lines, which were differentiated into cortical glutamatergic excitatory neurons using the Neurogenin-2 (Ngn2) protocol (Zhang et al., 2013). Using a wild-type unedited hESC line as a control, we performed molecular- and cellular-based characterizations at two different developmental time points representing neuronal maturation and synapse formation (day 7 and day 28, respectively) in induced neurons (iNs). Consistent with CASK's reported role in dendritic morphogenesis, using transcriptomics and morphology analysis, we found that immature excitatory iNs (day 7) showed an increased dendritic complexity and upregulation of gene networks related to neuronal cell adhesion, neurite outgrowth, and cytoskeletal organization. Upon neuronal maturity and well into synapse development, mature excitatory iNs lacking *CASK* showed defects in neuronal spiking and synchronized neuronal network firing patterns without significant changes in neuronal morphology and synapse numbers. Whole-cell patch-clamp electrophysiology measurements revealed that *CASK* LOF in iNs results in a selective decrease in the frequency of spontaneous excitatory postsynaptic currents (sEPSCs), which suggests a presynaptic defect. In agreement with this result, DEG analysis from bulk RNA-seq in day 28 iNs revealed significant changes in gene regulatory networks associated with synaptic function. Remarkably, the comparative analysis of our day 28 transcriptomic data with a recently published transcriptomic dataset by Becker et al. (2020) showed a significant overlap of DEGs induced by *CASK* mutations across genetic backgrounds, thus revealing a core set of genes that are commonly affected by *CASK* mutations.

In summary, while CASK functions to stabilize dendritic outgrowth in the developing human cortical excitatory neurons, subsequently, CASK plays a pivotal role in the regulation of synaptic release and establishment of cortical excitatory neuronal networks without directly influencing synapse formation. These results highlight the multi-faceted roles of CASK during neuronal maturation and synapse development and the value of human neuronal models of *CASK* deficiency in elucidating the molecular and cellular mechanisms underlying *CASK*-related syndromes.

RESULTS

Generation of isogenic *CASK* KO human embryonic stem cell lines and differentiation into cortical excitatory induced neurons

As *CASK* is an X-linked gene, we chose to perform gene editing in a male control pluripotent stem cell line to create a complete LOF model. Using H1 hESCs as the parental line, we introduced a plasmid (lenti-CRISPR v2) expressing Cas9 and *CASK*-specific guide RNAs (sgRNAs) targeting the first coding exon via nucleofection (Figure 1A). Transient selection by puromycin allowed the propagation of hESCs that carried this construct. Upon replating this edited pool, we established single cell clones, which were screened by PCR amplification and Sanger sequencing (Figure 1B). Through this method, we established two independent *CASK* null cell lines (KO1 and KO2), representing 14-bp and 10-bp deletions that disrupt the first coding exon and cause a frameshift. Although some residual transcripts of *CASK* could be detected at the mRNA level (Tables S1, S4, related to Figure 2), these mutations resulted in a complete LOF for CASK protein as verified by immunoblotting (Figure 1C). Both KO1 and KO2 hESCs were able to differentiate efficiently into cortical excitatory iNs by Ngn2 forced expression (Zhang et al., 2013) and were chosen for subsequent molecular and cellular analyses (Figure 1D).

Differential gene expression networks in *CASK* KO immature induced neurons

As CASK has been shown to function both as an early neurodevelopmental effector and a late synaptic organizer (Hsueh, 2009), we first chose an early development time point (day 7) in iNs, without the presence of supporting mouse glial cells (Zhang et al., 2013), to investigate the neurodevelopmental effects of *CASK* LOF in human cortical excitatory neurons. Taking total RNA from each differentiated cell line, we performed bulk RNA-seq to examine the potential differences in gene expression programs between WT and KO genotypes in early developing iNs. Four independent culture replicates from WT, KO1 and KO2 were used for this analysis. Through differential gene expression analysis using DESeq2 ((Love et al., 2014); cutoff of FC $\geq$ 1.2 or FC $\leq$ 0.8, p $\leq$ 0.05; minimum of 5 TPM per gene), we found a total of 876 DEGs (420 up-regulated, 456 down-regulated) that were common across two *CASK* KO lines compared to WT (Figure 2A, Table S1). Unbiased gene set enrichment analysis (GSEA; ToppGene (Chen et al., 2009)) revealed enrichment in specific and related gene ontology (GO) terms (Bonferroni correction of $p < 0.05$ as the threshold for significant GO terms) with a significant number of up-regulated DEGs concentrated on cell adhesion (GO:0034330; p value 5.85E-06), cell projection and morphogenesis (GO:0032990; p value 9.60E-07), neuronal development (GO:0048666; p value 1.26E-05), and synaptic membrane/structure (GO:0097060; p value 1.56E-08) (Figure 2B, Table S2). This pattern of enrichment was far more minimal in the down-regulated DEGs (Figures S1, S2, Table S2, related to Figure 2).

To validate these results, we performed quantitative RT-PCR using probes against 25 up-regulated DEGs and 12 down-regulated DEGs from total RNA isolated from 4 to 5 independent culture samples per genotype. A vast majority of these DEGs were validated with statistical significance confirming these genes as target DEGs (Figures 2C, S1B). Among these targets, multiple synaptic genes (SynGO (Koopmans et al., 2019)) were validated including *SHANK1*, *SNCB*, *SYT3*, *PCDH8*, *PTPRT*, *NECTIN1*, *FEZ1*, *ROR2*, *APLP2*, *CNTN2*, *GDI1*, and *RPL10* (Table S3, related to Figure 2). In addition, genes related to cell adhesion and structural regulation (*PCDHGA10*, *CXCL12*, *NRK*, *ARHGAP32*, *PLXNB2*, and *LRP5*) and transcription (*ZNF737*, *ID1*, and *UBE2G1*) were also validated.

In addition, we performed protein-protein interaction (PPI) network analysis using ToppCluster (Chen et al., 2009) to examine which of the day 7 DEGs encode for protein interactors of CASK by focusing on primary (direct) and secondary (indirect) degree interactors. Of the DEGs represented in the PPI network, four proteins as direct interactors and 32 indirect interactors were found, suggesting that most dysregulated genes induced by *CASK* LOF consist of indirect interactors (Figure S3, Table S4, related to Figure 2). Among the direct interactors of CASK, TNIK, which encodes TRAF2- and NCK-interacting protein kinase, stood out as a major hub protein in the CASK PPI network (Figure S3, related to Figure 2). Interestingly, TNIK is an activator of the WNT signaling pathway and is recruited to the promoters of WNT target genes by phosphorylating TCF7L2 (Coba et al., 2012; Mahmoudi et al., 2009; Shitashige et al., 2010). Moreover, TNIK is part of a signaling complex consisting of NEDD4, RAP2A, and TNIK, which regulates dendritic extension and arborization during neuronal development (Kawabe et al., 2010). Based on TNIK's association with the WNT signaling pathway, we checked whether any other DEGs represented known regulators of the WNT pathway. Indeed, 8 DEGs (*WNT5A*, *RSPO3*, *RRM2*, *LRP5*, *KLH12*, *INVS*, *CSNK2B*, and *CSNK1E*), in addition to TNIK, were differentially expressed in *CASK* KO iNs. The directionality of the transcript changes

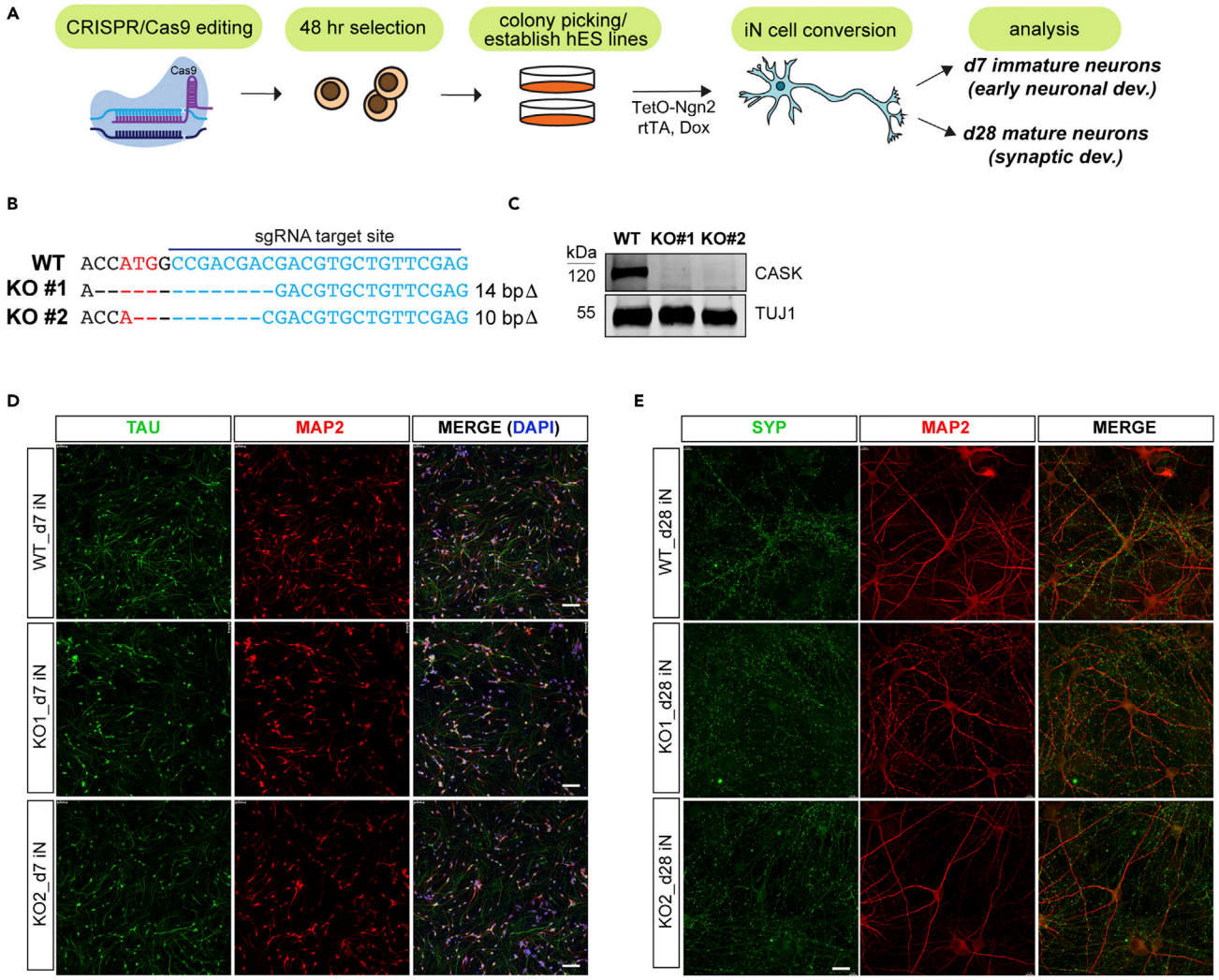

Figure 1. CRISPR-mediated generation of *CASK* KO hESC lines and differentiation into iN cells

(A) A schematic of workflow describing the generation of constitutive *CASK* KO hESC lines via CRISPR/Cas9, expansion of clonal cell lines, and Ngn2-iN cell differentiation. Analysis time points were on day 7 to assess early neuronal development and on day 28 to assess synaptic development.

(B) Verification of gene-edited genomic DNA sequence in the human *CASK* exon 1 by Sanger sequencing. sgRNA target region downstream of the ATG site (red) is noted. Resulting deletions obtained using CRISPR-mediated gene editing are shown.

(C) Immunoblot verification of complete *CASK* LOF on day 4 Ngn2-iN cells using an anti-CASK antibody. TUJ1 was used as a loading control.

(D) Representative confocal images of immunostained d7 immature iNs showing developing axons (TAU-green) and dendrites (MAP2-red) (scale bars, 100 μm).

(E) Representative confocal images of d28 iN cells immunostained with a presynaptic marker SYP (green) and a dendritic marker MAP2 (red) (scale bars, 20 μm).

correlated with a possible overactivated WNT signaling state (Table S1, related to Figure 2), which has been previously shown to promote dendritic overgrowth phenotype in cultured neurons (Rosso et al., 2005; Yu and Malenka, 2003). Taken together, these results show that there exists dysregulated neuronal organization in the absence of *CASK*, which highlights its cell-autonomous role in controlling early neuronal outgrowth and morphology.

CASK KO induced neurons display neurite overgrowth at an early stage of development

Normally, active neuronal outgrowth occurs in day 7 iNs, as they undergo dendritic and axonal outgrowth and exhibit gene expression profiles of immature, developing neurons (Chanda et al., 2019; Zhang et al., 2013). Compared to WT, day 7 iNs lacking *CASK* showed gene expression profiles indicative of neuronal

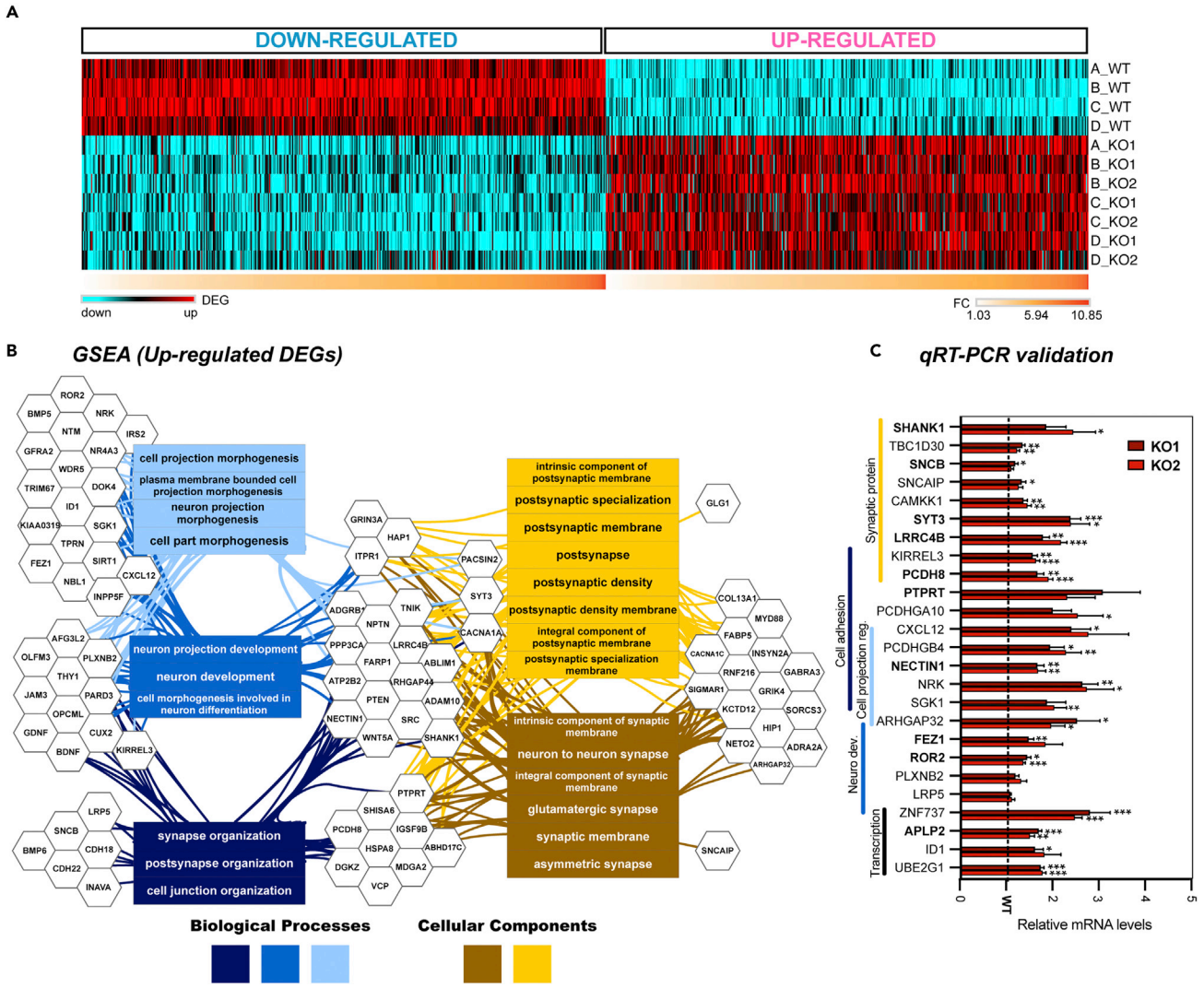

Figure 2. Differential gene expression analysis in d7 *CASK* KO immature iNs using bulk RNA sequencing

(A) Heatmap showing both up- and down-regulated DEGs across independent culture replicates (4 replicates for WT & KO1, 3 replicates for KO2). Cutoff for DEGs was set at FC $\geq$ 1.2 or $\leq$ 0.8, $p < 0.05$; minimum of 5 TPM per gene). A total of 876 shared DEGs were identified in *CASK* KO1 and KO2, as compared to WT control, with 420 genes up-regulated and 456 genes down-regulated.

(B) Gene set enrichment analysis (GSEA; ToppCluster) of commonly up-regulated DEGs (Bonferroni correction of $p < 0.05$ as the threshold for significant GO-terms) identified 83 DEGs localized into 6 major clusters and 4 small clusters or isolated DEGs, and enriched across 3 major Biological Processes (BP, in blue shades; cell projection morphogenesis, p value 9.60E-07; neurodevelopment, p value 1.26E-05; cell junction organization/adhesion, p value 5.85E-06) and 2 overlapping GO Cellular Components (CC, in yellow shades; synapse, p value 3.09E-06; postsynapse, p value 2.01E-08) affected by *CASK* LOF.

(C) qRT-PCR validation of specific up-regulated DEGs for both KO1 and KO2 relative to WT (set to 1). GAPDH probe was used as a normalization control. Bolded probes indicate genes cross-referenced with SynGO. Four independent replicates per genotype were validated, and each qRT-PCR experiment was performed in triplicate for 26 up-regulated DEGs. qRT-PCR data represent means $\pm$ SEM, and statistical analysis was performed using Student's *t* test comparing WT to each individual KO (*$p < 0.05$, **$p < 0.01$, ***$p < 0.001$; nonsignificant comparisons are not indicated).

overgrowth and increased complexity, which prompted us to examine their morphology. Using transient transfection on day 4, neurons were sparsely labeled with green fluorescent protein (GFP) expressed under a Synapsin promoter (SYN-EGFP vector). On day 7, upon fixation, we performed confocal imaging and neurite outgrowth analysis to measure various parameters as previously performed (Pak et al., 2015, 2021). Compared to WT, *CASK* KO iNs, indeed, showed an overall increase in total dendritic length and number of branch points without significant changes in soma size and the number of primary processes (Figures 3A and 3B). These results agree with gene expression data where, in the absence of *CASK*, iNs fail to restrict neuronal complexity and structural integrity.

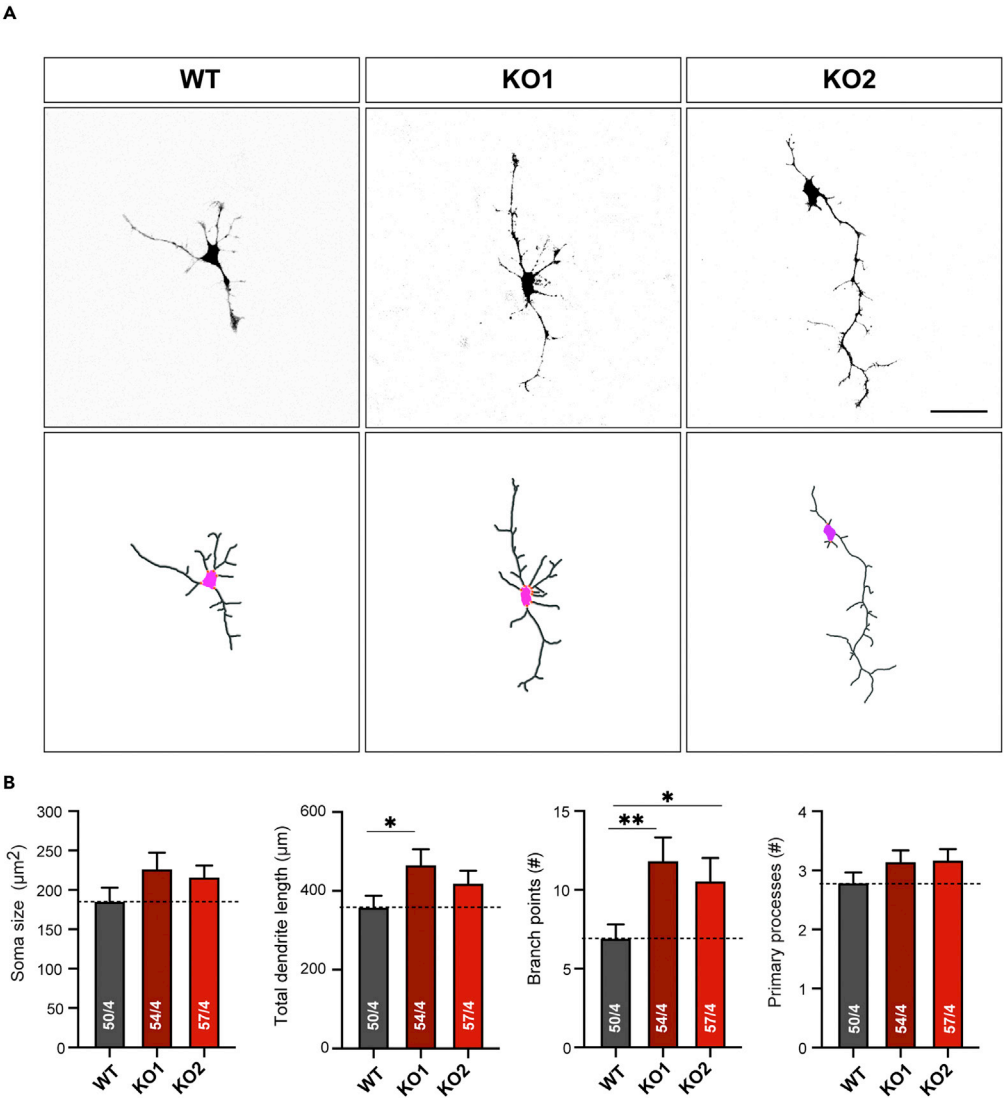

Figure 3. Quantification of neurite outgrowth for immature d7 *CASK* KO Ngn2-iNs shows an overgrowth phenotype

(A) Representative images (top) and binary mask (bottom) of day 7 Ngn2-iNs which were transfected with SYN-EGFP construct at day 4 to label single neurons for morphological quantification (scale bar, 50 µm).

(B) Quantification of morphological parameters in WT and KO1 and KO2 using Imaris (Bitplane). Summary graphs of soma size, total dendritic length, number of branch points, and number of primary processes. Data represent means ± SEM (numbers in bars represent # of cells/# of independent culture replicates performed). Statistical analysis was performed using Student's *t* test comparing WT to each individual KO (*$p < 0.05$, **$p < 0.01$; nonsignificant comparisons are not indicated).

Mature induced neurons lacking *CASK* exhibit normal neuronal and synaptic morphology

To understand the functional role of CASK in synaptic development in human cortical excitatory neurons, we co-cultured WT and *CASK* KO day 3 iNs with mouse glia and assayed neuronal morphology at day 28. This relatively mature time point is well-documented and displays active synaptic properties and elaborate neuronal morphology (Pak et al., 2021; Zhang et al., 2013). Similar to day 7 analysis, we transiently transfected developing iNs with SYN-EGFP plasmid at day 14 to sparsely label single neurons with EGFP and performed immunohistochemistry using antibodies against the presynaptic marker Synaptophysin (SYP) and the postsynaptic marker PSD95. By confocal imaging, we acquired images of single neurons at both 20X (to quantify neurite outgrowth) and focused dendritic segments at 60X (to quantify synapse numbers).

From four independent culture batches, we quantified various parameters, including soma size, total dendritic length, number of branch points, and number of primary processes for neurite analysis and synaptic density and volume for synapse analysis. As shown in Figure 4, there was no significant change in the parameters measured for neurite complexity except for a slight decrease in soma size for KO1 compared to WT (Figures 4A and 4B). Overall, the complexity of *CASK* KO iNs was similar to those of WT iNs, unlike what was observed in day 7 iNs. In synaptic puncta measurements, we found no difference in the density or the volume of SYP and PSD95 puncta on fixed dendritic segments, suggesting that synapse formation is not altered in *CASK* KO iNs (Figures 4C and 4D).

Decreased neuronal network activity in *CASK* KO mature induced neurons

To assay neuronal firing at the population level over two different time points (21 and 28 days post neuronal induction), we employed a CMOS-based high-density microelectrode array (MEA) system (Maxwell Biosystems) (Müller et al., 2015). In this experimental set-up, we co-cultured WT or *CASK* KO day 3 iNs with mouse glia on the MEA chips and recorded neuronal activity over two developmental time points, day 21 and day 28. As shown in Figures 5, S4, S5, and S6, WT iNs showed robust neuronal firing activity as measured by spike firing rates and amplitudes on days 21 and 28. The spike amplitude increased over time from 60 to 90 μV, indicating the strengthening of these neuronal connections over maturation (Figures 5B and S5B). In addition to spike activity, WT iNs displayed a consistent level of synchrony as evidenced by the network bursts (Figures 5C, S5C), which increased in duration over 7 days (0.8 s on day 21; 1.3 s on day 28). In *CASK* KO iNs, we observed an overall decrease in the firing rate and amplitude of these neuronal spikes on both days 21 and 28, indicating decreased neuronal firing and strength (Figures 5, S5). In addition, the burst frequency, representing neuronal network synchronicity, was significantly lower at both time points with an inverse correlation in inter-burst intervals (Figures 5C, S5C). All other measures of synchrony, such as mean burst duration, burst peak firing rate, and spikes per burst remained unaltered, indicating the composition of synchronized bursts was the same (Figure S6, related to Figure 5). Of all the neuronal spikes detected during the recording, there were also fewer spikes occurring inside the bursts themselves, which was consistent across both time points (Figures 5C, S5C). Significantly, these firing patterns were observed in two independent *CASK* KO lines and were not due to differences in neuronal plating or active area of the recording chips (Figure S4, related to Figure 5). Altogether, these results indicate that although the neuronal morphology and synapse formation are not altered, the strength of these connections as well as their network synchronicity are compromised in *CASK* KO iNs.

Defects in synaptic transmission and neuronal excitability in *CASK* KO mature induced neurons

We speculated that the observed decreases in MEA spike activity frequency and amplitude could be due to defects in coupling neurotransmitter release machinery and calcium channels at the active zone, as previously documented for CASK (Maximov and Bezprozvanny, 2002; Olsen et al., 2005). This prompted us to examine the properties of synaptic transmission at a single-cell level using whole-cell patch-clamp electrophysiology (Maximov et al., 2007). Based on the MEA data, we hypothesized that *CASK* LOF would result in a reduction of synaptic release in these iN cultures. Under voltage clamp configuration, we recorded spontaneous postsynaptic excitatory currents (sEPSCs) in WT and *CASK* KO iNs (KO1 & KO2). *CASK* KO iNs showed a profound decrease in the frequency of sEPSCs but not the amplitude (Figures 6, S7). Combined with synaptic morphology data, in which synapse number was unchanged, this result indicates there is likely an overall decrease in the probability of neurotransmitter release in *CASK* KO iN cultures.

We next investigated the intrinsic membrane properties and action potential (AP) parameters in iNs generated from the isogenic *CASK* KO and control under a current clamp configuration. Overall, *CASK* KO iNs did not show statistically significant changes in intrinsic membrane properties (resting membrane potential and capacitance) as well as spontaneous AP kinetics and composition (Figures S8, S9, related to Figure 6). *CASK* KO1 iNs specifically, but not KO2, showed a slight increase in the input resistance (Figure S8A, related to Figure 6). The increase in input resistance could be attributed to fewer membrane proteins, including ion channels. We then tested their ability to generate APs. No obvious changes were found in the *CASK* KO iNs in the major parameters for APs (Figures S8B, S9B, related to Figure 6), suggesting that the LOF of *CASK* likely does not impact the development of voltage-dependent sodium channels as well as potassium channels (two major channels responsible for determining the kinetics of APs). However, in both *CASK* KO1 and KO2 iNs, the excitability of these cells was increased, showing a decrease in the current injection necessary to depolarize the cell membrane (i.e. $V_m = I_{inj}*R_{in}$) (Figures S8C, S9C, related

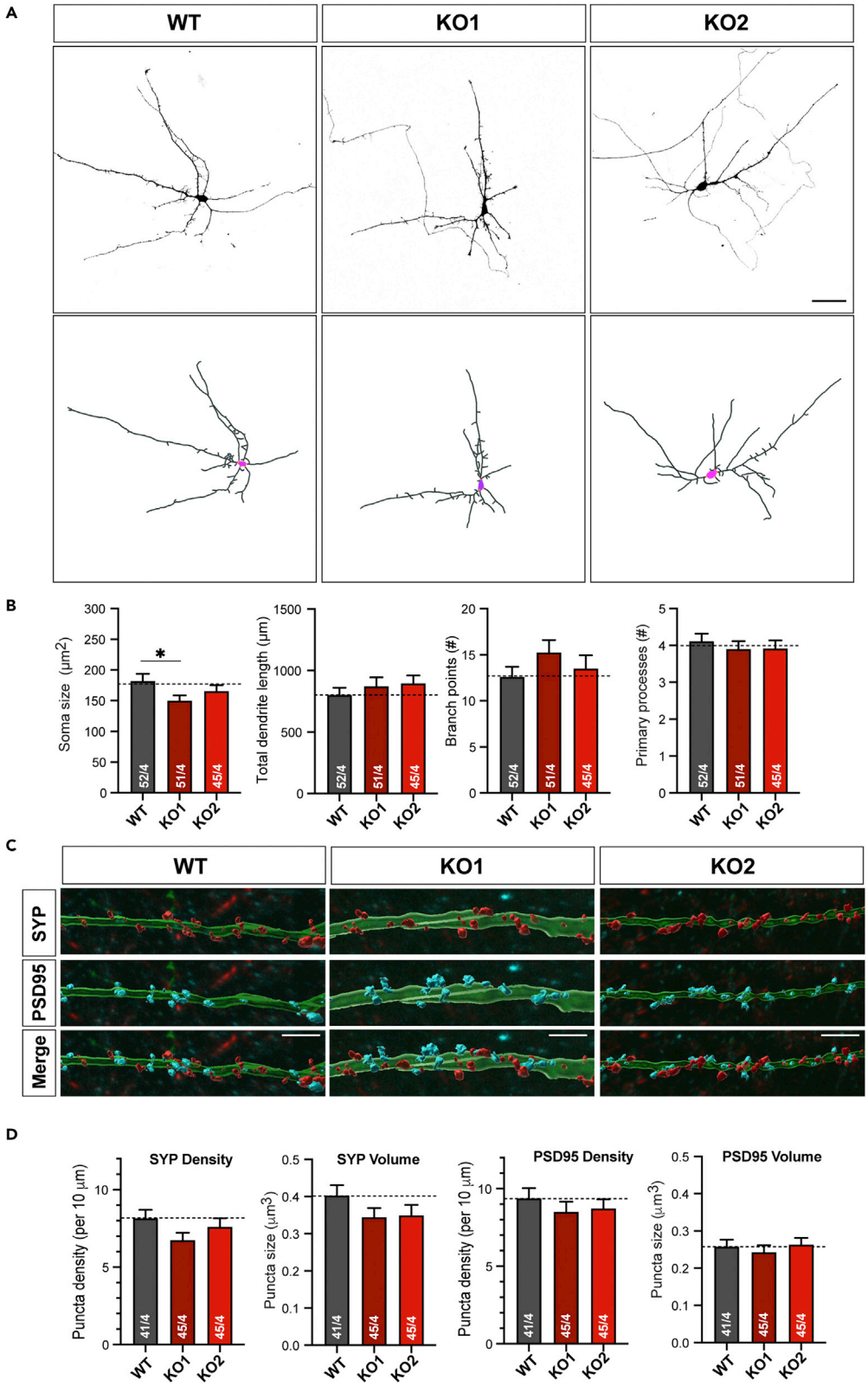
A
WT
KO1
KO2
B
Soma size (μm2)
Total dendrite length (μm)
Branch points (#)
Primary processes (#)
52/4
51/4
45/4
C
SYP
PSD95
Merge
D
SYP Density
SYP Volume
PSD95 Density
PSD95 Volume
Puncta density (per 10 μm)
Puncta size (μm3)
41/4
45/4

Figure 4. Dendritic arborization and synaptic puncta formation are unchanged in mature day 28 *CASK* KO iNs

(A) Representative images (top) and binary mask (bottom) of iN cultures that were sparsely transfected with SYN-EGFP at day 14 and grown to maturity (day 28) (scale bar, 50 μm).

(B) Quantification summary graphs of soma size, total dendritic length, number of branch points, and number of primary processes.

(C) Binary mask overlay of representative confocal images showing MAP2+ dendritic segments with presynaptic (SYP, in red) and postsynaptic (PSD95, in cyan) markers (scale bar, 5 μm).

(D) Quantification of morphological parameters in WT and KO1 and KO2 using Imaris (Bitplane). Summary graphs of presynaptic (SYP) and postsynaptic (PSD95) puncta density and synapse volume. Data represent means ± SEM (numbers in bars represent # of cells/# of independent culture replicates performed). Statistical analysis was performed using Student's *t* test comparing WT to each individual KO.

to Figure 6). The increased excitability could occur from homeostatic changes induced by reduced synaptic strengths (Figures 6, S7) and the overall reduced synchrony of firing in the neuronal network (Figure 5).

In conclusion, based on the results from both whole-cell patch-clamp electrophysiology and MEA measurements, there exists a dominant synaptic deficit associated with *CASK* LOF, which is driving the decreases in synaptic transmission and network activity. The slight increase in neuronal excitability phenotype cannot compensate for the synaptically driven responses, indicating a potential secondary deficit.

Differential gene expression networks in *CASK* KO mature induced neurons

Given the electrophysiological phenotypes seen in mature *CASK* KO iNs at both the population and single-cell level, we investigated the transcriptomic changes associated with *CASK* LOF using bulk RNA sequencing, similar to our day 7 approach. In day 28 cultures, owing to the presence of both human iNs and mouse glia, we used previously implemented computational methods to bioinformatically separate human iNs from mouse glial cells, allowing us to identify changes in gene expression specific to human iNs (Pak et al., 2021). A total of 12 samples were processed and sequenced from four independent cultures collected from WT, KO1, and KO2. Using DESeq2 (Love et al., 2014) (FC $\geq$ 1.2 or FC $\leq$ 0.8, p $\leq$ 0.05; minimum of 5 TPM per gene), we identified a total of 1742 DEGs (906 up-regulated, 838 down-regulated) that were commonly dysregulated in both KO1 and KO2 compared to WT (Figure 7A, Table S5). A number of DEGs (214 out of 1742) were synaptically localized genes that mapped to unique SynGO annotated genes, with many assigned to both presynaptic and postsynaptic functions (Koopmans et al., 2019) (Figure 7B, Table S7). In line with the decrease in spontaneous synaptic transmission seen in *CASK* KO iNs (Figures 6, S7), multiple genes regulating synaptic vesicle release were identified as significant DEGs (*VAMP2/SYB2*, *STX1B*, *SYT2*, *RIMBP2*, *RAB3A*, *CPLX1*) (Figures 7B and 7C). In addition, postsynaptic cell adhesion molecules, neurotransmitter receptors, and signaling molecules (*GRIA2*, *GRIA3*, *GABRA3*, *GABRA5*, *CBLN2*, *SLITRK3-4*, *LRRTM1-3*, *MAP2K1*, *PAK3*, *STAT3*) as well as the components of the ubiquitin-proteasome system (*TRIM3*, *NEDD4*, *UBE2A*) were identified as DEGs (Figures 7B and 7C), indicating a combinatorial dysregulation of both pre- and post-synaptic gene regulatory networks owing to *CASK* LOF. Interestingly, previously identified *CASK* targets, *RELN* (WT vs. KO1 & KO2) and NMDA-receptor type subunit (*GRIN1*; for WT vs. KO1) (Hsueh et al., 2000; Wang et al., 2004a, 2004b) were found to be differentially regulated, further validating these genes as hits. Additionally, we performed GSEA using either the total DEG gene set (pooled up- and down-regulated) or separated DEG subsets (up-regulated or down-regulated) using ToppGene (Chen et al., 2009) (Figures 7D, S10, Table S6). Here, we separately validated an enrichment of Biological Processes and Cellular Components involved in synapse organization (GO:0050808; p value 5.65E-15), assembly (GO:0007416; p value 1.86E-08), and synaptic signaling (GO:0099538; p value 4.56E-08) (Figures 7D, S10). DEGs related to neuronal projection development (GO:0048812; p value 2.43E-14), cellular morphogenesis (GO:0000902; p value 6.53E-18), and neuronal apoptosis (GO:0070997; p value 1.03E-06) were also enriched (Figures 7D, S10), despite the normal neuronal and synaptic morphology seen in the *CASK* KO iNs (Figure 4). Enrichment analysis of day 28 DEGs within the CASK PPI network showed a modest number of primary (direct) and secondary (indirect) protein interactors of CASK (Figure S11, Table S9, related to Figure 7).

We next performed a direct comparison of our day 28 DEGs with a recently published transcriptomic dataset from human neurons differentiated from iPSCs derived from two *CASK* mutation carriers (Becker et al., 2020). Two patients were both genetically and clinically distinct - a male individual who carried a splice site mutation in *CASK* was diagnosed with ASD and a female individual with intellectual disability carried an exonic duplication in *CASK*. To investigate whether there exists a shared set of core DEGs that could

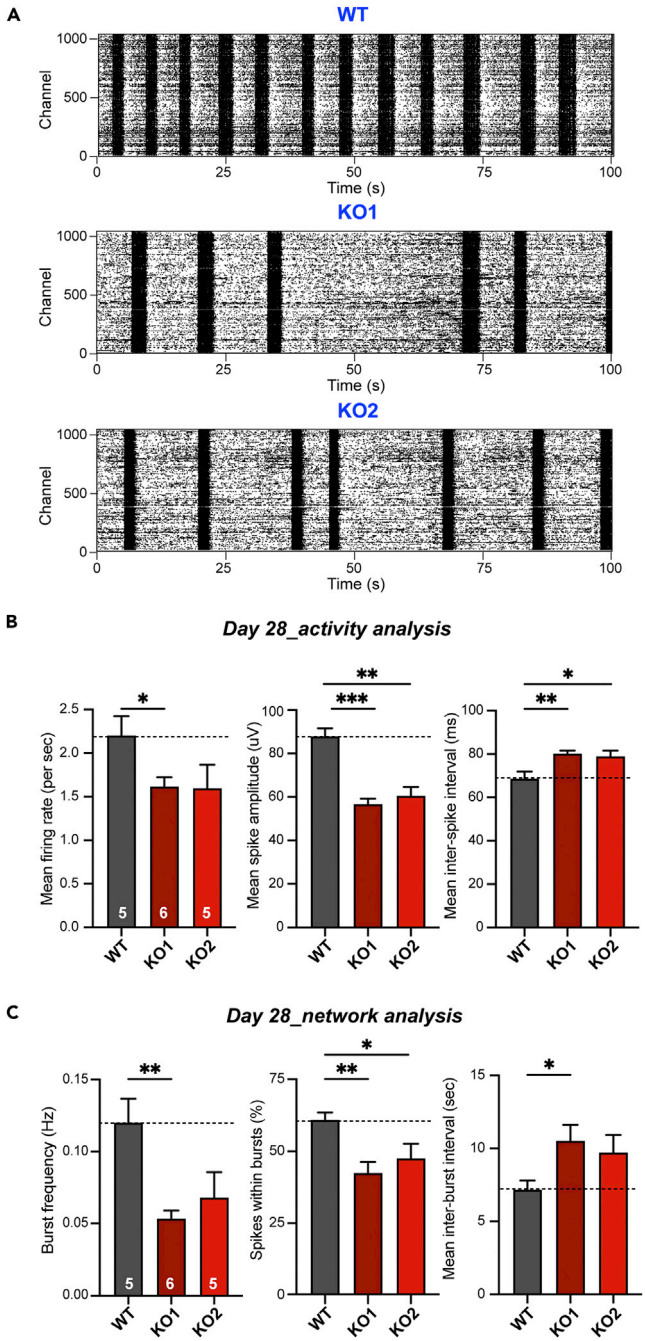

Figure 5. Measurements of synchronous neuronal activity for *CASK* KO mature iNs using high-density microelectrode arrays

(A) Representative raster plots showing decreased network activity for day 28 *CASK* KO iNs as compared to WT. Y axis represents # of active recording channels and X axis represents time in seconds (s).

(B) Analysis of spike activity revealed a significant decrease in mean firing rate (Hz) and mean spike amplitude (μV), as well as an increase in the mean inter-spike interval (ms) for *CASK* KO neuronal networks across both cell lines.

(C) Analysis of network activity indicated a significant decrease in burst frequency (Hz), aligning with an increase in mean inter-burst intervals, and a decrease in the percentage of spikes within bursts in *CASK* KO neurons as compared to WT. Data represent means ± SEM (numbers in bars represent # of independent culture replicates performed). Statistical analysis was performed using Student's *t* test comparing WT to each individual KO (*$p < 0.05$, **$p < 0.01$, ***$p < 0.001$; nonsignificant comparisons are not indicated).

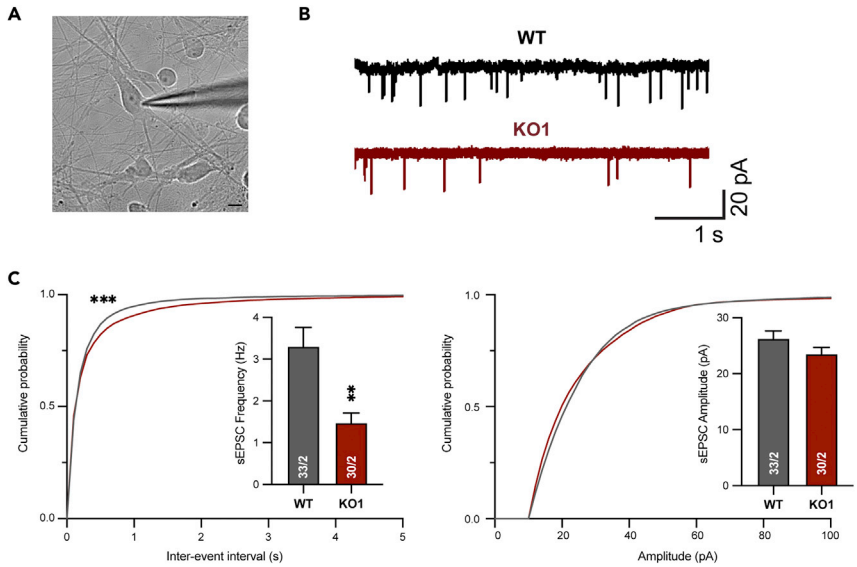

Figure 6. Mature *CASK* KO neurons exhibit a significant decrease in the frequency of spontaneous excitatory synaptic events but no change in amplitude

(A) Representative DIC image of mature iN cells co-cultured with mouse glia with a patch pipette attached to the cell body of the neuron. Electrophysiological recordings in cultured iN cells were performed in the whole-cell patch-clamp configuration (scale bar, 10 μm).

(B) Representative traces of sEPSC recordings.

(C) Left, cumulative probability plot of inter-event intervals and summary graphs of the sEPSC frequency. Right, cumulative probability plot and summary graphs of the sEPSC amplitude. Data represent means ± SEM (numbers in bars represent # of cells/# of independent culture replicates performed). Statistical analyses were performed by Student's *t* test for the bar graphs and by Kolmogorov-Smirnov tests for cumulative probability plots, comparing *CASK* KO1 with control WT neurons (*p < 0.05, **p < 0.01, ***p < 0.001; nonsignificant comparisons are not indicated). All recordings were performed between days 23 and 28.

potentially drive *CASK* LOF phenotypes across genetic backgrounds, we searched for overlaps between the two DEG datasets. A total of 232 DEGs were identified as overlapping DEGs (DEG criteria of adjusted p values < 0.05 and absolute log2 FC > 0.5, see STAR Methods), including those involved in synaptic cell adhesion (*CBLN2*, *CNTN4*, *LRRTM3*, *KIRREL3*, *SLITRK4*), cell adhesion (*PCDHA2*, *PCDHGA2*, *PCDHGB5*, *CDH13*, *EFNB1*), vesicle release (*SYP*, *SYT2*, *SYTL5*, *MCTP1*), and WNT signaling (*TCF7L2*, *ROR2*, *NKD1*, *DKK2*) (Table S8, related to Figure 7). Enrichment analysis using the CASK PPI network revealed that 69 out of 227 protein-coding DEGs fall within this network, with a majority being indirect interactors (Figure S12, Table S9, related to Figure 7). These results highlight that across genetic backgrounds, *CASK* mutations in mature human neurons induce transcriptional changes in both direct and indirect interactors of CASK, as well as regulators of synaptic function.

DISCUSSION

Herein, we investigated both the neurodevelopmental and synaptic roles of *CASK* using human excitatory iN KO models. In an early neuronal growth phase (day 7), we observed an increase in the overall gene expression profiles related to neurite outgrowth, projection morphogenesis, and cell adhesion from transcriptomic analysis and confirmed these changes in morphology as evidenced by increases in neurite length and the number of branch points (Figure 3). Interestingly, among the DEGs in day 7 transcriptomic analysis, regulators of the WNT signaling pathway were identified (Figure S3, Table S1, related to Figure 2). Besides its critical role in embryonic patterning and cell specification, WNT signaling regulates neuronal maturation and function by controlling axon and dendrite outgrowth, synaptic function, and plasticity (Ciani et al., 2011; Rosso and Inestrosa, 2013; Rosso et al., 2005; Yu and Malenka, 2003). In the future, it will be informative to test whether the inhibition of WNT can reverse the dendritic overgrowth phenotype in *CASK* LOF iNs and if WNT agonist treatment in WT iNs can phenocopy *CASK* LOF.

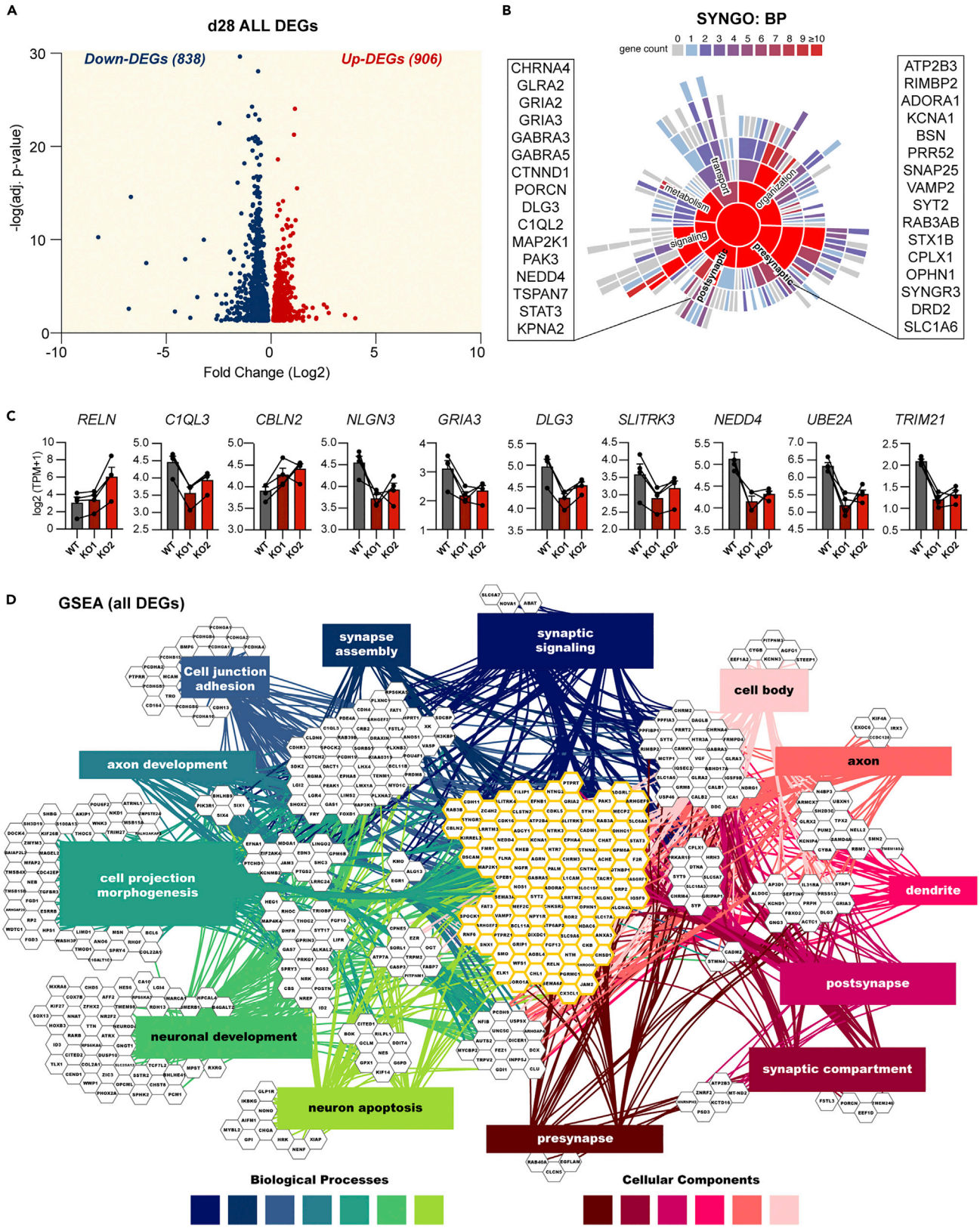
A
d28 ALL DEGs
Down-DEGs (838)
Up-DEGs (906)
-log(adj. p-value)
Fold Change (Log2)
B
SYNGO: BP
gene count
0 1 2 3 4 5 6 7 8 9 ≥10
CHRNA4
GLRA2
GRIA2
GRIA3
GABRA3
GABRA5
CTNND1
PORCN
DLG3
C1QL2
MAP2K1
PAK3
NEDD4
TSPAN7
STAT3
KPNA2
transport
organization
metabolism
signaling
postsynaptic
presynaptic
ATP2B3
RIMBP2
ADORA1
KCNA1
BSN
PRR52
SNAP25
VAMP2
SYT2
RAB3AB
STX1B
CPLX1
OPHN1
SYNGR3
DRD2
SLC1A6
C
RELN
C1QL3
CBLN2
NLGN3
GRIA3
DLG3
SLITRK3
NEDD4
UBE2A
TRIM21
log2 (TPM+1)
WT
KO1
KO2
D
GSEA (all DEGs)
synapse assembly
synaptic signaling
Cell junction adhesion
cell body
axon development
axon
cell projection morphogenesis
dendrite
postsynapse
neuronal development
synaptic compartment
neuron apoptosis
presynapse
Biological Processes
Cellular Components

Figure 7. Differential gene expression analysis in d28 *CASK* KO mature iNs using bulk RNA sequencing

(A) Volcano plot showing -log (adjusted p value) and log2 (fold change) for overlapping DEGs common in *CASK* KO cell lines compared to WT which met the cutoff for FC $\geq$ 1.2 or FC $\leq$ 0.8, p $\leq$ 0.05 with a minimum of 5 TPM per gene. Paired DEG analysis performed by DESeq2 pipeline (see SI for details). 905 up-regulated DEGs (red) and 838 down-regulated DEGs (blue) were chosen for gene set enrichment analysis (GSEA) using ToppCluster and SynGO. All DEGs except *TMSB4X* (log2 FC of −0.58, adj. p value of 0.0003) were included in the Volcano plot.

(B) SynGO-based synaptic gene enrichment analysis identified 214 unique SynGO annotated genes out of 1742 total DEGs. 156 genes have a Biological Process annotation, and 189 genes have a Cellular Component annotation. 10 Cellular Component terms are significantly enriched at 1% FDR (testing terms with at least three matching input genes), with 5 for Biological Processes. Selected genes pertaining to presynapse and postsynapse are highlighted on either side.

(C) log 2(TPM+1) across culture replicates are shown for a selected number of representative DEGs.

(D) GSEA (ToppCluster) of overlapping DEGs (FC $\geq$ 1.5 or FC $\leq$ 0.5, p $\leq$ 0.05 with a minimum of 5 TPM per gene) in *CASK* KO1 and KO2 compared to WT (Bonferroni p < 0.05) identified 422 enriched DEGs, localized into 16 major clusters and 5 minor clusters across 7 major Biological Processes (BP, in blue shades; synaptic signaling, p value 4.56E-08; synapse assembly, p value 1.86E-08; cell junction adhesion, p value 5.56E-07; axon development, p value 7.43E-11; cell projection morphogenesis, p value 1.88E-14; neuronal development, p value 4.52E-12; neuronal apoptosis, p value 2.81E-07) and 6 Cellular Components (CC, in red shades; presynapse, p value 2.27E-06; synaptic compartment, p value 9.18E-15; postsynapse, p value 2.33E-07; dendrite, p value 1.35E-08; axon, p value 2.54E-10; neuronal cell body, p value 1.69E-07) affected by *CASK* LOF. DEGs from the central cluster highlighted in yellow were found to be enriched in all biological processes and cellular components.

Upon co-culturing these human iNs with mouse glia, a culturing scheme that promotes synaptogenesis (Pak et al., 2015; Zhang et al., 2013), we investigated the effects of *CASK* KO on excitatory synaptic transmission (day 28). As indicated by its previously established protein-protein interactions with neurotransmitter release machinery, voltage-gated calcium channels, and the cell adhesion molecule neurexin at presynaptic terminals (Butz et al., 1998; Hata et al., 1996; Maximov and Bezprozvanny, 2002; Mukherjee et al., 2008), *CASK* KO iNs showed a prominent decrease in the frequency of sEPSCs without changes in neuronal morphology and synapse number (Figures 4 and 6, S7). This result indicated that the regulation of neurotransmitter release is comprised in *CASK* KO iNs. In particular, the synaptic observed during whole-cell patch-clamp electrophysiology experiments was supported by changes in synchronous firing activity measured by MEA recordings (Figures 5, S5, and S6). Indeed, in *CASK* KO iNs, there was an overall decrease in the neuronal spike activity (frequency and amplitude) as well as a decrease in the burst frequency and the percentage of spikes within bursts, indicating that synaptic deficits are driving changes in the network-level synchronicity. Although we observed minor changes in neuronal excitability and input resistance (Figures S8, S9, related to Figure 6), these parameters are most likely secondary, as these changes cannot compensate for the synaptically driven responses seen at both population and single-cell levels (Figures 5 and 6, S7). Interestingly, this phenotype is in line with our previous studies in heterozygous *NRXN1* cKO iNs, in which a similar decrease in excitatory synaptic function without changes in morphology was observed (Pak et al., 2015, 2021), suggesting that *CASK* LOF functionally mirrors the presynaptic defects driven by *NRXN1* heterozygosity in excitatory iN cells.

In agreement with electrophysiological phenotypes, day 28 bulk RNA-seq analysis of *CASK* LOF revealed an enrichment of biological functions related to synaptic assembly, synaptic signaling, and cellular components associated with pre- and post-synaptic compartments (Figure 7). Previously, in rodent models, *Cask* has been shown to regulate transcriptional levels of *Reln* and NMDAR subunit *NR2b* (Hsueh et al., 2000; Mori et al., 2019; Wang et al., 2004a, 2004b), suggesting its role as a transcriptional regulator for target genes important for neurodevelopment. In our transcriptomic data, we also detected an upregulation of *RELN* (~2-fold increase) in both *CASK* KO1 and KO2 iNs compared to WT on day 28 (Figure 7). Additionally, *GRIN1*, which encodes the NMDAR type subunit 1, was up-regulated (~1.3-fold increase) in *CASK* KO1 iNs compared to day 28 WT iNs. The reproducibility of these *CASK* targets in iNs is encouraging, and our transcriptomic data provides a developmental timing-specific (day 7 and 28) road map of direct and indirect *CASK* targets at the transcriptional level.

Importantly, from a comparative analysis of two transcriptomic datasets (our day 28 DEGs vs. DEGs found in Becker et al., 2020), we identified a set of overlapping DEGs (Table S8, related to Figure 7). Despite using different human pluripotent stem cell lines harboring *CASK* mutations (isogenic *CASK* LOF hESCs in this study vs. iPSCs derived from two distinct patients with unique *CASK* mutations in Becker et al., 2020) and different neuronal differentiation protocols (pure cortical excitatory neurons in this study vs. mixed cortical excitatory/inhibitory neurons in Becker et al., 2020), we found 227 overlapping DEGs between the datasets. From this analysis, it is clear that *CASK* dysfunction induces significant transcriptional changes in genes important for human cortical excitatory development and synaptic function regardless of genetic backgrounds. Follow-up studies investigating these shared DEGs will be helpful in identifying downstream

effectors of *CASK* LOF. In addition, DEGs specific to the patients and therefore, not shared with isogenic *CASK* KO iNs, can potentially reveal disease genetic background effectors.

Limitations of the study

A limitation of the current work is the lack of inhibitory input in the neuronal culture model for this study. As Ngn2-iN cells are purely excitatory (Zhang et al., 2013), mixing cultures of both excitatory and inhibitory neurons (Yang et al., 2017) could allow for the investigation of excitatory-inhibitory (E-I) balance, which is an important underlying mechanism for ASDs and intellectual disability (Rubenstein and Merzenich, 2003). In two mouse models, E-I imbalance has been documented in *Cask* mutants, showing an increase in spontaneous miniature excitatory postsynaptic currents and a decrease in spontaneous miniature inhibitory postsynaptic currents (Atasoy et al., 2007; Mori et al., 2019). Mechanistically, the observed E-I imbalance is attributed in part to NMDARs, as re-expression of *NR2b* restores the E-I balance (Mori et al., 2019). Interestingly, a decrease in inhibitory synaptic puncta density was specifically seen in iPSC-neurons derived from an ASD individual with *CASK* splice site mutation (Becker et al., 2020). Altogether, these studies show that E-I balance could potentially be disrupted in *CASK* LOF in human cells.

From a disease perspective, it will be interesting to test E-I balance in a *CASK* mutant context from both multiple isogenic and diverse disease backgrounds to study the genetic interactions between *CASK* variants and common variants, which will likely influence the expressivity of phenotypes mediated by *CASK* deficiency. Owing to the small sample size of engineered cell lines examined here, additional isogenic lines representing various control genetic backgrounds will increase the power of *CASK* LOF analysis. The addition of both male and female genetic backgrounds would also be useful in this case, as *CASK* LOF in males causes more severe phenotypes than females and results in early lethality (Moog et al., 2015).

Having established robust phenotypes associated with the cell-autonomous function of CASK in human excitatory neurons, future biochemical and functional studies in diverse cell types can add to this work, thereby providing a more comprehensive understanding of various cell types at play. For instance, there are non-neuronal functions of CASK, which need to be considered in future studies. Though CASK expression has been reported in glial cell types, like astrocytes and oligodendrocytes (Anitei et al., 2006; Zhang et al., 2014), our understanding of this molecule in these cell types is currently lacking. Testing whether specific intracellular binding partnerships exist in glial cells compared to neurons might be worth investigating. Beyond brain cell types, CASK expression and function have also been implicated in multiple tissue types, including intestinal epithelial cells, kidneys, and pancreas, implicating complex CASK biology in various organ systems (Ahn et al., 2013; Hata et al., 1996; Stevenson et al., 2000; Yan et al., 2007; Zhu et al., 2014).

STAR★METHODS

Detailed methods are provided in the online version of this paper and include the following:

- KEY RESOURCES TABLE
- RESOURCE AVAILABILITY
  - Lead contact
  - Materials availability
  - Data and code availability
- EXPERIMENTAL MODEL AND SUBJECT DETAILS
- METHOD DETAILS
  - Gene targeting
  - Generation of iN cells from human ESCs
  - Lentivirus production
  - Primary glia culture
  - Sparse transfection in iN cells
  - Immunohistochemistry
  - Bulk RNA sequencing and differential gene expression analysis
  - Quantitative RT-PCR
  - Immunoblotting
  - High-density microelectrode array (HD-MEA) network electrophysiology
  - Preparation of MEA chips
  - Whole-cell patch-clamp single-cell electrophysiology

- QUANTIFICATION AND STATISTICAL ANALYSIS
  - Whole-cell patch-clamp single-cell electrophysiology analysis
  - Image acquisition and quantification of neurite outgrowth and synaptic puncta
  - Bulk RNA-sequencing and differential gene expression analysis
  - Gene set enrichment analysis (GSEA) for both d7 and d28
  - CASK PPI network enrichment analysis for both d7 and d28

SUPPLEMENTAL INFORMATION

Supplemental information can be found online at https://doi.org/10.1016/j.isci.2022.105187.

ACKNOWLEDGMENTS

This work was supported by NIMH (R01MH122519 to C.P., R01MH125528 to Z.P.P.), UMass IALS/BMB faculty start-up fund (to C.P.), Tourette Association of America (Young Investigator Award to C.P.), and NIGMS T32 BTP training program (T32 GM135096 to D.M.). We thank Dr. Louise Giam for guidance with CRISPR/Cas9 gene editing and UMass IALS core facilities: Genomics (Dr. Ravi Ranjan) for bulk RNA sequencing assistance and light microscopy (Dr. Jim Chambers). We also thank members of the Pak lab, Dr. Adolfo Cuadra and Le Wang for fruitful discussion and intellectual support on electrophysiology measurements and Narciso Pavon for assistance with MEA analysis. Neurons in graphical abstract were created with BioRender.com.

AUTHOR CONTRIBUTIONS

C.P. generated CRISPR-engineered cell lines. D.M. performed all experiments pertaining to iN cell differentiation, morphology analysis, RNA work, and electrophysiology. R.G. performed image analysis, and K.J. analyzed RNA-seq data. D.M., Z.P.P., B.A., and C.P. took part in experimental design and data interpretation. D.M. and C.P. wrote the article.

DECLARATION OF INTERESTS

The authors declare no competing interests.

INCLUSION AND DIVERSITY

One or more of the authors of this paper self-identifies as a gender minority in their field of research. One or more of the authors of this paper self-identifies as a member of the LGBTQIA + community.

Received: March 17, 2022
Revised: August 30, 2022
Accepted: September 20, 2022
Published: October 21, 2022

REFERENCES

Ahn, S.-Y., Kim, Y., Kim, S.T., Swat, W., and Miner, J.H. (2013). Scaffolding proteins DLG1 and CASK cooperate to maintain the nephron progenitor population during kidney development. J. Am. Soc. Nephrol. *24*, 1127–1138. https://doi.org/10.1681/ASN.2012111074.

Anitei, M., Ifrim, M., Ewart, M.-A., Cowan, A.E., Carson, J.H., Bansal, R., and Pfeiffer, S.E. (2006). A role for Sec8 in oligodendrocyte morphological differentiation. J. Cell Sci. *119*, 807–818. https://doi.org/10.1242/jcs.02785.

Atasoy, D., Schoch, S., Ho, A., Nadasy, K.A., Liu, X., Zhang, W., Mukherjee, K., Nosyreva, E.D., Fernandez-Chacon, R., Missler, M., et al. (2007). Deletion of CASK in mice is lethal and impairs synaptic function. Proc. Natl. Acad. Sci. USA *104*, 2525–2530. https://doi.org/10.1073/pnas.0611003104.

Becker, M., Mastropasqua, F., Reising, J.P., Maier, S., Ho, M.-L., Rabkina, I., Li, D., Neufeld, J., Ballenberger, L., Myers, L., et al. (2020). Presynaptic dysfunction in CASK-related neurodevelopmental disorders. Transl. Psychiatry *10*, 312. https://doi.org/10.1038/s41398-020-00994-0.

Bray, N.L., Pimentel, H., Melsted, P., and Pachter, L. (2016). Near optimal probabilistic RNA-seq quantification. Nat. Biotechnol. *34*, 525–527.

Butz, S., Okamoto, M., and Südhof, T.C. (1998). A tripartite protein complex with the potential to couple synaptic vesicle exocytosis to cell adhesion in brain. Cell *94*, 773–782. https://doi.org/10.1016/s0092-8674(00)81736-5.

Chanda, S., Ang, C.E., Lee, Q.Y., Ghebrial, M., Haag, D., Shibuya, Y., Wernig, M., and Südhof, T.C. (2019). Direct reprogramming of human neurons identifies marcksl1 as a pathogenic mediator of valproic acid-induced teratogenicity. Cell Stem Cell *25*, 103–119.e6. https://doi.org/10.1016/j.stem.2019.04.021.

Chao, H.-W., Hong, C.-J., Huang, T.-N., Lin, Y.-L., and Hsueh, Y.-P. (2008). SUMOylation of the MAGUK protein CASK regulates dendritic spinogenesis. J. Cell Biol. *182*, 141–155. https://doi.org/10.1083/jcb.200712094.

Chen, C., and Okayama, H. (1987). High-efficiency transformation of mammalian cells by plasmid DNA. Mol. Cell Biol. *7*, 2745–2752. https://doi.org/10.1128/mcb.7.8.2745.

Chen, K., and Featherstone, D.E. (2011). Pre and postsynaptic roles for Drosophila CASK. Mol. Cell. Neurosci. *48*, 171–182. https://doi.org/10.1016/j.mcn.2011.07.009.

Chen, J., Bardes, E.E., Aronow, B.J., and Jegga, A.G. (2009). ToppGene Suite for gene list enrichment analysis and candidate gene prioritization. Nucleic Acids Res. *37*, W305–W311. https://doi.org/10.1093/nar/gkp427.

Ciani, L., Boyle, K.A., Dickins, E., Sahores, M., Anane, D., Lopes, D.M., Gibb, A.J., and Salinas, P.C. (2011). Wnt7a signaling promotes dendritic spine growth and synaptic strength through Ca^{2+}/Calmodulin-dependent protein kinase II. Proc. Natl. Acad. Sci. USA *108*, 10732–10737. https://doi.org/10.1073/pnas.1018132108.

Coba, M.P., Komiyama, N.H., Nithianantharajah, J., Kopanitsa, M.V., Indersmitten, T., Skene, N.G., Tuck, E.J., Fricker, D.G., Elsegood, K.A., Stanford, L.E., et al. (2012). TNiK is required for postsynaptic and nuclear signaling pathways and cognitive function. J. Neurosci. *32*, 13987–13999. https://doi.org/10.1523/JNEUROSCI.2433-12.2012.

Dobin, A., Davis, C.A., Schlesinger, F., Drenkow, J., Zaleski, C., Jha, S., Batut, P., Chaisson, M., and Gingeras, T.R. (2013). STAR: ultrafast universal RNA-seq aligner. Bioinformatics *29*, 15–21. https://doi.org/10.1093/bioinformatics/bts635.

Durinck, S., Moreau, Y., Kasprzyk, A., Davis, S., De Moor, B., Brazma, A., and Huber, W. (2005). BioMart and Bioconductor: a powerful link between biological databases and microarray data analysis. Bioinformatics *21*, 3439–3440.

Durinck, S., Spellman, P.T., Birney, E., and Huber, W. (2009). Mapping identifiers for the integration of genomic datasets with the R/Bioconductor package biomaRt. Nat. Protoc. *4*, 1184–1191.

Froyen, G., Van Esch, H., Bauters, M., Hollanders, K., Frints, S.G.M., Vermeesch, J.R., Devriendt, K., Fryns, J.-P., and Marynen, P. (2007). Detection of genomic copy number changes in patients with idiopathic mental retardation by high-resolution X-array-CGH: important role for increased gene dosage of XLMR genes. Hum. Mutat. *28*, 1034–1042. https://doi.org/10.1002/humu.20564.

Hata, Y., Butz, S., and Südhof, T.C. (1996). CASK: a novel dlg/PSD95 homolog with an N-terminal calmodulin-dependent protein kinase domain identified by interaction with neurexins. J. Neurosci. *16*, 2488–2494.

Hodge, J.J.L., Mullasseril, P., and Griffith, L.C. (2006). Activity-dependent gating of CaMKII autonomous activity by Drosophila CASK. Neuron *51*, 327–337. https://doi.org/10.1016/j.neuron.2006.06.020.

Hsueh, Y.-P. (2009). Calcium/calmodulin-dependent serine protein kinase and mental retardation. Ann. Neurol. *66*, 438–443. https://doi.org/10.1002/ana.21755.

Hsueh, Y.P., Wang, T.F., Yang, F.C., and Sheng, M. (2000). Nuclear translocation and transcription regulation by the membrane-associated guanylate kinase CASK/LIN-2. Nature *404*, 298–302. https://doi.org/10.1038/35005118.

Kawabe, H., Neeb, A., Dimova, K., Young, S.M., Takeda, M., Katsurabayashi, S., Mitkovski, M., Malakhova, O.A., Zhang, D.-E., Umikawa, M., et al. (2010). Regulation of Rap2A by the ubiquitin ligase Nedd4-1 controls neurite development. Neuron *65*, 358–372. https://doi.org/10.1016/j.neuron.2010.01.007.

Koopmans, F., van Nierop, P., Andres-Alonso, M., Byrnes, A., Cijsouw, T., Coba, M.P., Cornelisse, L.N., Farrell, R.J., Goldschmidt, H.L., Howrigan, D.P., et al. (2019). SynGO: an evidence-based, expert-curated knowledge base for the synapse. Neuron *103*, 217–234.e4. https://doi.org/10.1016/j.neuron.2019.05.002.

LaConte, L.E.W., Chavan, V., Liang, C., Willis, J., Schönhense, E.M., Schoch, S., and Mukherjee, K. (2016). CASK stabilizes neurexin and links it to liprin-α in a neuronal activity-dependent manner. Cell. Mol. Life Sci. *73*, 3599–3621. https://doi.org/10.1007/s00018-016-2183-4.

Li, B., and Dewey, C.N. (2011). RSEM: accurate transcript quantification from RNA-Seq data with or without a reference genome. BMC Bioinformatics *12*, 323. https://doi.org/10.1186/1471-2105-12-323.

Lin, Y.-L., Lei, Y.-T., Hong, C.-J., and Hsueh, Y.-P. (2007). Syndecan-2 induces filopodia and dendritic spine formation via the neurofibromin-PKA-Ena/VASP pathway. J. Cell Biol. *177*, 829–841. https://doi.org/10.1083/jcb.200608121.

Love, M.I., Huber, W., and Anders, S. (2014). Moderated estimation of fold change and dispersion for RNA-seq data with DESeq2. Genome Biol. *15*, 550. https://doi.org/10.1186/s13059-014-0550-8.

Lu, C.S., Hodge, J.J.L., Mehren, J., Sun, X.X., and Griffith, L.C. (2003). Regulation of the Ca2+/CaM-responsive pool of CaMKII by scaffold-dependent autophosphorylation. Neuron *40*, 1185–1197.

Mahmoudi, T., Li, V.S.W., Ng, S.S., Taouatas, N., Vries, R.G.J., Mohammed, S., Heck, A.J., and Clevers, H. (2009). The kinase TNIK is an essential activator of Wnt target genes. EMBO J. *28*, 3329–3340. https://doi.org/10.1038/emboj.2009.285.

Maximov, A., and Bezprozvanny, I. (2002). Synaptic targeting of N-type calcium channels in hippocampal neurons. J. Neurosci. *22*, 6939–6952. https://doi.org/10.1523/JNEUROSCI.22-16-06939.2002.

Maximov, A., Pang, Z.P., Tervo, D.G.R., and Südhof, T.C. (2007). Monitoring synaptic transmission in primary neuronal cultures using local extracellular stimulation. J. Neurosci. Methods *161*, 75–87. https://doi.org/10.1016/j.jneumeth.2006.10.009.

Moog, U., Bierhals, T., Brand, K., Bautsch, J., Biskup, S., Brune, T., Denecke, J., de Die-Smulders, C.E., Evers, C., Hempel, M., et al. (2015). Phenotypic and molecular insights into CASK-related disorders in males. Orphanet J. Rare Dis. *10*, 44. https://doi.org/10.1186/s13023-015-0256-3.

Mori, T., Kasem, E.A., Suzuki-Kouyama, E., Cao, X., Li, X., Kurihara, T., Uemura, T., Yanagawa, T., and Tabuchi, K. (2019). Deficiency of calcium/calmodulin-dependent serine protein kinase disrupts the excitatory-inhibitory balance of synapses by down-regulating GluN2B. Mol. Psychiatry *24*, 1079–1092. https://doi.org/10.1038/s41380-018-0338-4.

Mukherjee, K., Sharma, M., Urlaub, H., Bourenkov, G.P., Jahn, R., Südhof, T.C., and Wahl, M.C. (2008). CASK Functions as a Mg2+-independent neurexin kinase. Cell *133*, 328–339. https://doi.org/10.1016/j.cell.2008.02.036.

Müller, J., Ballini, M., Livi, P., Chen, Y., Radivojevic, M., Shadmani, A., Viswam, V., Jones, I.L., Fiscella, M., Diggelmann, R., et al. (2015). High-resolution CMOS MEA platform to study neurons at subcellular, cellular, and network levels. Lab Chip *15*, 2767–2780. https://doi.org/10.1039/c5lc00133a.

Najm, J., Horn, D., Wimplinger, I., Golden, J.A., Chizhikov, V.V., Sudi, J., Christian, S.L., Ullmann, R., Kuechler, A., Haas, C.A., et al. (2008). Mutations of CASK cause an X-linked brain malformation phenotype with microcephaly and hypoplasia of the brainstem and cerebellum. Nat. Genet. *40*, 1065–1067. https://doi.org/10.1038/ng.194.

Olsen, O., Moore, K.A., Fukata, M., Kazuta, T., Trinidad, J.C., Kauer, F.W., Streuli, M., Misawa, H., Burlingame, A.L., Nicoll, R.A., and Bredt, D.S. (2005). Neurotransmitter release regulated by a MALS-liprin-alpha presynaptic complex. J. Cell Biol. *170*, 1127–1134. https://doi.org/10.1083/jcb.200503011.

Pak, C., Danko, T., Zhang, Y., Aoto, J., Anderson, G., Maxeiner, S., Yi, F., Wernig, M., and Südhof, T.C. (2015). Human neuropsychiatric disease modeling using conditional deletion reveals synaptic transmission defects caused by heterozygous mutations in nrxn1. Cell Stem Cell *17*, 316–328. https://doi.org/10.1016/j.stem.2015.07.017.

Pak, C., Danko, T., Mirabella, V.R., Wang, J., Liu, Y., Vangipuram, M., Grieder, S., Zhang, X., Ward, T., Huang, Y.-W.A., et al. (2021). Cross-platform validation of neurotransmitter release impairments in schizophrenia patient-derived NRXN1-mutant neurons. Proc. Natl. Acad. Sci. USA *118*, e2025598118. https://doi.org/10.1073/pnas.2025598118.

Patel, P.A., Liang, C., Arora, A., Vijayan, S., Ahuja, S., Wagley, P.K., Settlage, R., LaConte, L.E.W., Goodkin, H.P., Lazar, I., et al. (2020). Haploinsufficiency of X-linked intellectual disability gene CASK induces post-transcriptional changes in synaptic and cellular metabolic pathways. Exp. Neurol. *329*, 113319. https://doi.org/10.1016/j.expneurol.2020.113319.

Piluso, G., Carella, M., D'Avanzo, M., Santinelli, R., Carrano, E.M., D'Avanzo, A., D'Adamo, A.P., Gasparini, P., and Nigro, V. (2003). Genetic heterogeneity of FG syndrome: a fourth locus (FGS4) maps to Xp11.4-p11.3 in an Italian family. Hum. Genet. *112*, 124–130. https://doi.org/10.1007/s00439-002-0863-7.

Rosso, S.B., and Inestrosa, N.C. (2013). WNT signaling in neuronal maturation and synaptogenesis. Front. Cell. Neurosci. *7*, 103. https://doi.org/10.3389/fncel.2013.00103.

Rosso, S.B., Sussman, D., Wynshaw-Boris, A., and Salinas, P.C. (2005). Wnt signaling through Dishevelled, Rac and JNK regulates dendritic development. Nat. Neurosci. *8*, 34–42. https://doi.org/10.1038/nn1374.

Rubenstein, J.L.R., and Merzenich, M.M. (2003). Model of autism: increased ratio of excitation/inhibition in key neural systems. Genes Brain Behav. *2*, 255–267. https://doi.org/10.1034/j.1601-183x.2003.00037.x.

Shannon, P., Markiel, A., Ozier, O., Baliga, N.S., Wang, J.T., Ramage, D., Amin, N., Schwikowski, B., and Ideker, T. (2003). Cytoscape: a software environment for integrated models of biomolecular interaction networks. Genome Res. *13*, 2498–2504. https://doi.org/10.1101/gr.1239303.

Shitashige, M., Satow, R., Jigami, T., Aoki, K., Honda, K., Shibata, T., Ono, M., Hirohashi, S., and Yamada, T. (2010). Traf2- and nck-interacting kinase is essential for Wnt signaling and colorectal cancer growth. Cancer Res. *70*, 5024–5033. https://doi.org/10.1158/0008-5472.CAN-10-0306.

Soneson, C., Love, M.I., and Robinson, M.D. (2015). Differential analyses for RNA-seq: transcript-level estimates improve gene-level inferences. F1000Res. *4*, 1521. https://doi.org/10.12688/f1000research.7563.2.

Spangler, S.A., Schmitz, S.K., Kevenaar, J.T., de Graaff, E., de Wit, H., Demmers, J., Toonen, R.F., and Hoogenraad, C.C. (2013). Liprin-α2 promotes the presynaptic recruitment and turnover of RIM1/CASK to facilitate synaptic transmission. J. Cell Biol. *201*, 915–928. https://doi.org/10.1083/jcb.201301011.

Srivastava, S., McMillan, R., Willis, J., Clark, H., Chavan, V., Liang, C., Zhang, H., Hulver, M., and Mukherjee, K. (2016). X-linked intellectual disability gene CASK regulates postnatal brain growth in a non-cell autonomous manner. Acta Neuropathol. Commun. *4*, 30. https://doi.org/10.1186/s40478-016-0295-6.

Stevenson, D., Laverty, H.G., Wenwieser, S., Douglas, M., and Wilson, J.B. (2000). Mapping and expression analysis of the human CASK gene. Mamm. Genome *11*, 934–937. https://doi.org/10.1007/s003350010170.

de Vries, B.B.A., Breedveld, G.J., Deelen, W.H., Breuning, M.H., Niermeijer, M.F., and Heutink, P. (2002). Another family with nonspecific X-linked mental retardation (Mrx78) maps to Xp11.4-p11.23. Am. J. Med. Genet. *111*, 443–445. https://doi.org/10.1002/ajmg.10576.

Wang, G.-S., Hong, C.-J., Yen, T.-Y., Huang, H.-Y., Ou, Y., Huang, T.-N., Jung, W.-G., Kuo, T.-Y., Sheng, M., Wang, T.-F., and Hsueh, Y.P. (2004a). Transcriptional modification by a CASK-interacting nucleosome assembly protein. Neuron *42*, 113–128. https://doi.org/10.1016/s0896-6273(04)00139-4.

Wang, T.-F., Ding, C.-N., Wang, G.-S., Luo, S.-C., Lin, Y.-L., Ruan, Y., Hevner, R., Rubenstein, J.L.R., and Hsueh, Y.-P. (2004b). Identification of Tbr-1/CASK complex target genes in neurons. J. Neurochem. *91*, 1483–1492. https://doi.org/10.1111/j.1471-4159.2004.02845.x.

Yan, Y., Vasudevan, S., Nguyen, H., Bork, U., Sitaraman, S., and Merlin, D. (2007). Extracellular interaction between hCD98 and the PDZ class II domain of hCASK in intestinal epithelia. J. Membr. Biol. *215*, 15–26. https://doi.org/10.1007/s00232-007-9001-8.

Yang, N., Chanda, S., Marro, S., Ng, Y.-H., Janas, J.A., Haag, D., Ang, C.E., Tang, Y., Flores, Q., Mall, M., et al. (2017). Generation of pure GABAergic neurons by transcription factor programming. Nat. Methods *14*, 621–628. https://doi.org/10.1038/nmeth.4291.

Yu, X., and Malenka, R.C. (2003). β-catenin is critical for dendritic morphogenesis. Nat. Neurosci. *6*, 1169–1177. https://doi.org/10.1038/nn1132.

Yukselen, O., Turkyilmaz, O., Ozturk, A.R., Garber, M., and Kucukural, A. (2020). DolphinNext: a distributed data processing platform for high throughput genomics. BMC Genomics *21*, 310. https://doi.org/10.1186/s12864-020-6714-x.

Zhang, Y., Pak, C., Han, Y., Ahlenius, H., Zhang, Z., Chanda, S., Marro, S., Patzke, C., Acuna, C., Covy, J., et al. (2013). Rapid single-step induction of functional neurons from human pluripotent stem cells. Neuron *78*, 785–798. https://doi.org/10.1016/j.neuron.2013.05.029.

Zhang, Y., Chen, K., Sloan, S.A., Bennett, M.L., Scholze, A.R., O'Keeffe, S., Phatnani, H.P., Guarnieri, P., Caneda, C., Ruderisch, N., et al. (2014). An RNA-sequencing transcriptome and splicing database of glia, neurons, and vascular cells of the cerebral cortex. J. Neurosci. *34*, 11929–11947. https://doi.org/10.1523/JNEUROSCI.1860-14.2014.

Zhu, Z.-Q., Wang, D., Xiang, D., Yuan, Y.-X., and Wang, Y. (2014). Calcium/calmodulin-dependent serine protein kinase is involved in exendin-4-induced insulin secretion in INS-1 cells. Metabolism *63*, 120–126. https://doi.org/10.1016/j.metabol.2013.09.009.

Zordan, M.A., Massironi, M., Ducato, M.G., Te Kronnie, G., Costa, R., Reggiani, C., Chagneau, C., Martin, J.-R., and Megighian, A. (2005). Drosophila CAKI/CMG protein, a homolog of human CASK, is essential for regulation of neurotransmitter vesicle release. J. Neurophysiol. *94*, 1074–1083. https://doi.org/10.1152/jn.00954.2004.

STAR★METHODS

KEY RESOURCES TABLE

REAGENT or RESOURCE	SOURCE	IDENTIFIER
Antibodies		
Rabbit anti-Synaptophysin primary antibody	Abcam	RRID: ab14692
Mouse anti-PSD-95 primary antibody	Invitrogen	Cat.#: MA1-046; RRID: AB_2092361
Chicken anti-MAP2 primary antibody	Abcam	RRID: ab5392
Mouse anti-TAU primary antibody	Invitrogen	Cat.#: MN1000; RRID: AB_2314654
Chicken anti-GFP primary antibody	Aves	Cat.#: GFP-1010; RRID: AB_2307313
Goat anti-Mouse 488 secondary antibody	Thermo Fisher	Cat.#: A-11001; RRID: AB_2534069
Goat anti-Mouse 546 secondary antibody	Thermo Fisher	Cat.#: A-11003; RRID: AB_2534071
Goat anti-Mouse 647 secondary antibody	Thermo Fisher	Cat.#: A-21236; RRID: AB_2535805
Goat anti-Chicken 488 secondary antibody	Thermo Fisher	Cat.#: A-11039; RRID: AB_2534096
Goat anti-Chicken 546 secondary antibody	Thermo Fisher	Cat.#: A-11040; RRID: AB_2534097
Goat anti-Chicken 647 secondary antibody	Thermo Fisher	Cat.#: A-21449; RRID: AB_2535866
Goat anti-Rabbit 488 secondary antibody	Thermo Fisher	Cat.#: A-11034; RRID: AB_2576217
Goat anti-Rabbit 546 secondary antibody	Thermo Fisher	Cat.#: A-11010; RRID: AB_2534077
Goat anti-Rabbit 647 secondary antibody	Thermo Fisher	Cat.#: A-21245; RRID: AB_2535813
Mouse anti-CASK	Neuromab	Cat.#: 75–000; RRID: AB_2068730
Mouse anti-TUJ1/TUBB3	Biolegend	Cat.#: 801201; RRID: AB_2313773
Fluorescent secondary donkey anti-mouse antibody	Licor	Cat.#: 925-32212; RRID: AB_2716622
Bacterial and virus strains		
Top10 *E. coli* bacteria	Thermo Fisher	Cat.#: C404010
DH5α *E. coli* bacteria	Thermo Fisher	Cat.#: 18258012
pTet-O-**Ngn2**-puro LV	Produced in Pak lab	
FUW-M2**rtTA** LV	Produced in Pak lab	
Biological samples		
Goat serum	Gibco	Cat.#: 16-210-064
Fetal bovine serum (For neuronal media)	GE Life Sciences	Cat.#: SH3008803
Fetal bovine serum (For HEK media)	Sigma	Cat.#: F0926-500ML
Chemicals, peptides, and recombinant proteins		
Calcium chloride ($CaCl_2$)	Sigma	Cat.#: C5670-500G
Magnesium chloride ($MgCl_2$)	Sigma	Cat.#: M8266-100G
Sucrose	Sigma	Cat.#: S0389-1KG
DPBS	GIbco	Cat.#: 14190-250
Matrigel	Corning	Cat.#: 356235
TergaZyme	Alconox	Cat.#: Z273287
Trypan Blue	Thermo	Cat.#: 15250061
Paraformaldehyde (PFA)	Electron Microscopy Sciences	Cat.#: 1457141
Dimethyl sulfoxide (DMSO)	Sigma	Cat.#: D2650-5X5ML
Triton X-100	Sigma	Cat.#: T8787-250ML
Buffer RLT	Qiagen	Cat.#: 79216
β-mercaptoethanol	Sigma	Cat.#: M6250
Sodium chloride	Sigma	Cat.#: S9888-5KG

(*Continued on next page*)

Continued

REAGENT or RESOURCE	SOURCE	IDENTIFIER
Sodium phosphate dibasic	Sigma	Cat.#: S7907
HEPES	Sigma	Cat.#: H4034-100G
LB agar powder	Thermo	Cat.#: J75851-A1
Borate buffer	Thermo	Cat.#: 28341
Polyethyleneimine (PEI)	Sigma/Merck	Cat.#: P3143
Laminin	Sigma/Merck	Cat.#: L2020
K-Gluconate	Sigma	Cat.#: G4500-100G
Potassium chloride (KCl)	Sigma	Cat.#: P3911
ATP-Mg	Sigma	Cat.#: A9187-100MG
GTP-Na_2	Sigma	Cat.#: G8877-25MG
Phosphocreatine	Sigma	Cat.#: P7936-10MG
Carbon dioxide (^{13}C, 99%) (<2% ^{18}O)	Ivey	Cat.#: CA 8122
Papain	Worthington Biochemical Corporation	Cat.#: LS003127
EDTA	Sigma	Cat.#: E5134-1KG
RNase-free DNase	Qiagen	Cat.#: 79254
Fluoromount DAPI	Southern Biotech	Cat.#: 0100-20
$NaHCO_3$	Sigma	Cat.#: S6014-500G
Tris-HCl	Sigma	Cat.#: 1185531
cOmplete™, Mini Protease Inhibitor Cocktail	Sigma	Cat.#: 11836153001
Luteinizing broth powder	Sigma	Cat.#: L3022
mTeSR+ stem cell medium	Stem Cell Technologies	Cat.#: 100-0276
DMEM/F12 medium	Thermo Fisher	Cat.#: 11330057
Neurobasal medium	Thermo Fisher	Cat.#: 21103049
Minimal essential medium (MEM)	Thermo Fisher	Cat.#: 51-200-038
DMEM	Thermo Fisher	Cat.#: 11995-065
N2 supplement	Fisher	Cat.#: 17502048
B27 supplement	Fisher	Cat.#: 17504044
NEAA	Life Technologies	Cat.#: 11140-050
Glutamax	Life Technologies	Cat.#: 35050-061
BDNF	Peprotech	Cat.#: 450-02
NT-3	Peprotech	Cat.#: 450-03
Mouse laminin	Thermo Fisher (Life Technologies)	Cat.#: 23017-015
Doxycycline	Clontech	Cat.#: D9891-1G
A Cytosine β-D-arabinofuranoside hydrochloride (AraC)	Sigma	Cat.#: C6645-100MG
Transferrin	Gemini Bio	Cat.#: 800-131P
200 mM L-glutamine	Gibco	Cat.#: 25030081
Puromycin	Invivogen	Cat.#: ant-pr-1
Penicillin/Streptomycin	Gibco	Cat.#: 15140122
Ampicillin	Sigma	Cat.#: A9518-100G
Kanamycin	Sigma	Cat.#: K4000-50G
Y-27632 compound	Axon Medchem	Cat.#: 1683
Laminin (for HD-MEA chips)	Sigma	Cat.#: L2020
Trypsin-EDTA	Thermo Fisher	Cat.#: 25300062
ReLeSR dissociation reagent	Stem Cell Technologies	Cat.#: 05872
Accutase dissociation reagent	Innovative Cell Technologies	Cat.#: AT 104-500

(*Continued on next page*)

Continued

REAGENT or RESOURCE	SOURCE	IDENTIFIER
Critical commercial assays		
RNeasy RNA extraction kit	Qiagen	Cat.#: 74106
Taqman Fast Virus 1-Step Master Mix	Applied Biosystems	Cat.#: 4444432
Plasmid Midiprep kit	Qiagen	Cat.#: 12145
NEBNext Ultra Directional RNA Library Prep Kit for Illumina	New England Biolabs	Cat.#: E7420L
4D Nucleofector kit	Lonza	V4XP-3032
Deposited data		
Raw and processed bulk RNA-seq data	This paper	GEO: GSE199910
Expression profiling by high throughput sequencing	Becker et al. (2020)	GEO: GSE140572
Experimental models: Cell lines		
H1 wild type human male embryonic stem cell line	WiCell	Stem Cell Line Catalog ID: WA01
H1-6 CASK-KO human male embryonic stem cell line	Generated by Pak Lab	This paper
H1-23 CASK-KO human male embryonic stem cell line	Generated by Pak Lab	This paper
HEK293T human cells	ATCC	Cat.#: CRL-3216
Experimental models: Organisms/strains		
Primary mouse glial cells	Dissociated from postnatal day 0-2 CD1 mouse pups; adult pregnant mouse provided by Charles River Labs	Cat.#: C57BL/6NCrl
Oligonucleotides		
APBB3 qRT-PCR Probe: TGGAGAGTTC ACTGGACCGGAGT Forward primer: CCACCATACCAGGA CAGAGA Reverse primer: GGAACTAGGAGATG CAGAGGA	IDT	IDT Probe ID: Hs.PT.58.14944352
APLP2 qRT-PCR Probe: AAGAAG GAATGGGAAGAGGCAGAGC Forward primer: ATGGCTTGGAAGTGCTGAA Reverse primer: CGCAACCGAATGGACAGG	IDT	IDT Probe ID: Hs.PT.56a.23012253.g
ARHGAP32 qRT-PCR Probe: AAGAAC GTAATGAGCTTGCCGTGC Forward primer: CACAACCAAACAC CCTCTCT Reverse primer: GTGACCAACTCAGTGCCA	IDT	IDT Probe ID: Hs.PT.58.24732581
CAMKKI qRT-PCR Probe: CTGGGCCT CGAGTACTTGCACTG Forward primer: GATGGCTTGATGTCCCTGT Reverse primer: CAAGCTCGCCTCTACCTG	IDT	IDT Probe ID: Hs.PT.58.24877261
CNTN2 qRT-PCR Probe: TTCCAGTAGCGGATCTCATACCCCA Forward primer: TGCTGTCCTCACTCGGT Reverse primer: ATCCTCAGAGATGA ACGTGAC	IDT	IDT Probe ID: Hs.PT.58.4324417

(*Continued on next page*)

Continued

REAGENT or RESOURCE	SOURCE	IDENTIFIER
CXCL12 qRT-PCR Probe: CGTGCTGGTCCTCGTGCTGA Forward primer: CATCTGTAGCTCAG GCTGAC Reverse primer: CATGAACGCCAAGGTCGT	IDT	IDT Probe ID: Hs.PT.58.27881121
FEZ1 qRT-PCR Probe: CTGCCCTACCT AACCTTGCCCTTT Forward primer: CTGTGATGGAATGA CTCTTGCT Reverse primer: GTGCCTACTTTG CTAACGGA	IDT	IDT Probe ID: Hs.PT.58.26247608
GAPDH qRT-PCR Probe: CAGCAAGAGCACAAGAGGAAGAGAGA Forward primer: AGGGTGGTGGACCTCAT Reverse primer: TGAGTGTGGCAGGGACT	IDT	IDT Probe ID: Hs.PT.39a.22214836
GDI1 qRT-PCR Probe: CACAGACATGATG CCCGACAGGAT Forward primer: GGTGTGATGGAGG AGCTCT Reverse primer: CATGGACGAGGA ATACGATGT	IDT	IDT Probe ID: Hs.PT.58.39260001
GREM2 qRT-PCR Probe: ACCTTCACCA GCACCGCCA Forward primer: CTGCTGCCGTCCTTGTAAG Reverse primer: GCTTCCATCACGTCATTGC	IDT	IDT Probe ID: Hs.PT.58.38639879
ID1 qRT-PCR Probe: AGAATCTCCACCTT GCTCACCTTGC Forward primer: CCTGATGTAGTCGATG ACGTG Reverse primer: GCTGTTACTCACGC CTCAAG	IDT	IDT Probe ID: Hs.PT.58.18791272.g
KCNH2 qRT-PCR Probe: AGGACCTGGGT GACCTTCTCAGT Forward primer: GTGCCTGCAGCTTGTACT Reverse primer: CAGTGACCGTGAGAT CATAGC	IDT	IDT Probe ID: Hs.PT.58.1626479
KIRREL3 qRT-PCR Probe: CCGACTTCCAG ACCATCTACAACTGC Forward primer: TCCCGACTTCATTTCC GAAC Reverse primer: TGACCATCAGCAA CATCGTG	IDT	IDT Probe ID: Hs.PT.58.2537139
LRP5 qRT-PCR Probe: ACCTCTCTGAGC CAAGGCCAAAA Forward primer: GCTGTAGATGTCG ATGCTGAG Reverse primer: AGAACATCAAGCGAGCCAA	IDT	IDT Probe ID: Hs.PT.58.39397667
LRRC4B qRT-PCR Probe: CGTCCGGATCACC TGGATGCC Forward primer: GTTCTTGCTCAGCTGCAGA Reverse primer: CGGTACCTGAACCTGCAAG	IDT	IDT Probe ID: Hs.PT.58.3368993

(*Continued on next page*)

Continued

REAGENT or RESOURCE	SOURCE	IDENTIFIER
MAP2 qRT-PCR Probe: TCGCAGAGCAGGGAAGAGTGGTA Forward primer: CAGGAGACAGAGAT GAGAATTCC Reverse primer: CAGGAGTGATGGC AGTAGAC	IDT	IDT Probe ID: Hs.PT.58.25625979
NDRG4 qRT-PCR Probe: TATCCCC AACCACCAGCATCACG Forward primer: CCAGAGTCTGCCA TCTTCAG Reverse primer: GGTGCCCAATGCCAAGA	IDT	IDT Probe ID: Hs.PT.58.27569171
NECTIN1 qRT-PCR Probe: TACCACTG GACCACGCTAAATGGC Forward primer: CCTTGAAGAAGAG GGTTCTGTT Reverse primer: CCTGCAAAGCTGA TGCTAAC	IDT	IDT Probe ID: Hs.PT.58.22958787
NRK qRT-PCR Probe: CCAACAGCAAATT GACTCCCCACAAAG Forward primer: GCCTTTCCACTTCTGTCCAT Reverse primer: GAGTTCACTTCTGA GATCTGCT	IDT	IDT Probe ID: Hs.PT.58.24359732
OLIG2 qRT-PCR Probe: AGAAGCAAATGA CAGAGCCGGAGC Forward primer: CTTCAAGTCATCC TCGTCCAG Reverse primer: TGTTGATCTTGA GACGCAGC	This paper	Custom-designed using IDT ID: N005806.1.pt.OLIG2
PCDH8 qRT-PCR Probe: CTTTACC GCTGTCTTTGCCGCTG Forward primer: GAATCGCTGTCG TTGAAATCAC Reverse primer: CACTCCTTCAACA CCATTTCTG	IDT	IDT Probe ID: Hs.PT.58.3045235.g
PCDHGA10 qRT-PCR Probe: ACTTCTCCATTGGCACCTTCGTCC Forward primer: ACTTCAACAA TTGCGTGTCAG Reverse primer: GTGAGTGTTCCTG AGAATTTGC	IDT	IDT Probe ID: Hs.PT.58.24769527.g
PCDHGB4 qRT-PCR Probe: CCTCCAGTT CCAGCATCACCCT Forward primer: GCGTTGTCATTTA CATCACCAA Reverse primer: CGAGCAGAATCCA GAGTACA	IDT	IDT Probe ID: Hs.PT.58.25450847.g
PLXNB2 qRT-PCR Probe: TCACGGTGTCCAG GTTCTTGCC Forward primer: CCAGATTCCTGCATGGTCA Reverse primer: CCACGAGACAGATGTGAACTTC	IDT	IDT Probe ID: Hs.PT.58.3360678

(*Continued on next page*)

Continued

REAGENT or RESOURCE	SOURCE	IDENTIFIER
PPP2R5B qRT-PCR Probe: ACCACATCTTCCTCCGGTTCATCTATGA Forward primer: GATCTCCAGCAGCTCAGC Reverse primer: GCCTACATCCGCAAACAGT	IDT	IDT Probe ID: Hs.PT.58.23278757
PTPRT qRT-PCR Probe: TTGCGACTCAAG GTCCGATGCA Forward primer: AGTTCTCCTGCCAG ATCATTC Reverse primer: CACTCTGACTACAT CAATGCCA	IDT	IDT Probe ID: Hs.PT.58.4425659
ROR2 qRT-PCR Probe: CCTGAGCCGTTA TAGCACTGATGGT Forward primer: CTTGCCGTTCCTCT GTAATCC Reverse primer: GACGCTGCCAACTGCAT	IDT	IDT Probe ID: Hs.PT.58.22908006
RPL10 qRT-PCR Probe: CGAGACTTTGGGT ACGGCTTGTTCT Forward primer: TGTACTTATTGGC ACAAATTCGG Reverse primer: CACTGAAGATCCT GGTGTCG	IDT	IDT Probe ID: Hs.PT.58.26238282
SGK1 qRT-PCR Probe: CATGCCAAC ATCCTGACCAAGCC Forward primer: AGTCGTTCAGACCCATCCT Reverse primer: GTGAAGTGAGAGAG CCATGT	IDT	IDT Probe ID: Hs.PT.58.472315
SHANK1 qRT-PCR Probe: ACTTCTTCAACCCCGTCTTCGTGTG Forward primer: CGAGCTGCACATACTCCAG Reverse primer: TCCGATACAAGA CCCGAGTT	IDT	IDT Probe ID: Hs.PT.58.2729044
SLC6A15 qRT-PCR Probe: TGTGAACAAAGTTCTGCCACCACCT Forward primer: ATATTCAGTGCT TCCCTGTACC Reverse primer: TCTCAGTCTTTT CAGCAACCC	IDT	IDT Probe ID: Hs.PT.58.1422940
SNCAIP qRT-PCR Probe: TCCAACGA GATGCCCTGTTCTTGC Forward primer: CTGTTGCCATCC TGGTCTAC Reverse primer: AGCCATTGCAGAACTGAGT	IDT	IDT Probe ID: Hs.PT.58.26564199
SNCB qRT-PCR Probe: CCACTTCCTCTGGC TTCAGATCAGT Forward primer: TCCTCATAACTCTC CCCTTCT Reverse primer: CACAGGACTGGTGA AGAGG	IDT	IDT Probe ID: Hs.PT.58.2966297
SYT3 qRT-PCR Probe: CCCTCCACGATGT CCCTCCAGA Forward primer: GCTCCCCAAGATCTGCTTT Reverse primer: TCTATGACTTTGACC GCTTCTC	IDT	IDT Probe ID: Hs.PT.58.24526182

(*Continued on next page*)

Continued

REAGENT or RESOURCE	SOURCE	IDENTIFIER
TAZ qRT-PCR Probe: AGGTTCCAGATGTGGC GGAGTTTC Forward primer: TCCTTGGTGAAGCA GATGTC Reverse primer: CCAATCACCAGTCCTGCAT	IDT	IDT Probe ID: Hs.PT.58.40508253
TBC1D30 qRT-PCR Probe: CAATTGTGGGAA AGGGAACGGAGC Forward primer: ACGGTGTAATGT TGTAGGTGT Reverse primer: CTTCTGCAAAGC CATGAACTC	IDT	IDT Probe ID: Hs.PT.58.27768844
UBE2G1 qRT-PCR Probe: TCACCTGC TAATGTTGATGCTGCGA Forward primer: CTCCATTT CTATCTTCCCTCCA Reverse primer: AGTGTCATTTCTA TGCTGGCA	IDT	IDT Probe ID: Hs.PT.58.150520
ZNF322 qRT-PCR Probe: AAGATAG CATTCGTAACAAGAA AGACTCAAGACC Forward primer: CCTGATCCTGAC AATTTGACTTC Reverse primer: CTGAACTAGAGA CCTTTTGAAACC	IDT	IDT Probe ID: Hs.PT.58.423693
ZNF445 qRT-PCR Probe: CATGCCAT TGCACTCCAGCCTTG Forward primer: GCAGAAGAAT CACTTGAACCCA Reverse primer: GTGGACCGATTGTCGCT	IDT	IDT Probe ID: Hs.PT.58.21096651
ZNF737 qRT-PCR Probe: CCTGGTCTT CCTTGGTATTGTTGTCTCT Forward primer: TGCTCCAGACAGGTGATGA Reverse primer: CTGCACAGCGG AATTTATATAGG	IDT	IDT Probe ID: Hs.PT.58.15618125
ZNF775 qRT-PCR Probe: CCAGCTCCTGT GCCGTTGC Forward primer: TTCTCCTGCTTG ACCTTCATC Reverse primer: CGTTAACCTTAGC CACAAAGTC	IDT	IDT Probe ID: Hs.PT.58.39416083
CRISPR sgRNA targeting CASK: 5′-CACCGGGACATAGTATTTGAAAGAC-3′	IDT	
Recombinant DNA		
pTet-*O*-**Ngn2**-puro	Addgene	RRID: Addgene_52047
FUW-M2**rtTA**	Addgene	RRID: Addgene_20342
Tet-*O*-FUW-E**GFP**	Addgene	RRID: Addgene_30130
pMDLg/p**RRE**	Addgene	RRID: Addgene_12251
pRSV-**Rev**	Addgene	RRID: Addgene_12253
pMD2.G (aka **VSVG**)	Addgene	RRID: Addgene_12259
Lenti-CRISPv2 sgRNA construct	Addgene	RRID: Addgene_52961

(*Continued on next page*)

Continued

REAGENT or RESOURCE	SOURCE	IDENTIFIER
Software and algorithms		
NIS Elements-Advanced Research	Nikon	https://www.microscope.healthcare.nikon.com/products/software/nis-elements/nis-elements-advanced-research
Imaris software	Bitplane	https://imaris.oxinst.com
Prism 9.3.0	GraphPad	https://www.graphpad.com/scientific-software/prism/
Office Suite	Microsoft	https://www.microsoft.com/en-us/microsoft-365/products-apps-services
Cytoscape (v3.9.1)	National Resource for Network Biology	https://cytoscape.org
MATLAB R2021a	MathWorks	https://www.mathworks.com/products/matlab.html
Quantstudio 3 System and RQ Analysis System	Thermo Fisher	https://www.thermofisher.com/us/en/home/life-science/pcr/real-time-pcr/real-time-pcr-instruments/quantstudio-systems.html
Easy Electrophysiology (2.3.3)		https://www.easyelectrophysiology.com/home
ClampFit (9.02)	Molecular Devices	https://support.moleculardevices.com/s/article/Axon-pCLAMP-11-Electrophysiology-Data-Acquisition-Analysis-Software-Download-Page
Dolphin processing software suite	Yukselen et al. (2020)	https://github.com/UMMS-Biocore/dolphinnext
STAR (2.6.0c) alignment tool	Dobin et al. (2013)	https://code.google.com/archive/p/rna-star/
RSEM (v1.2.28)	Li and Dewey (2011)	http://deweylab.github.io/RSEM/
Kallisto (v0.46.0)	Bray et al. (2016)	https://github.com/pachterlab/kallisto
tximport package (v1.16.1)	Soneson et al. (2015)	https://bioconductor.org/packages/release/bioc/html/tximport.html
DESeq2 (v1.28.1)	Love et al. (2014)	https://bioconductor.org/packages/release/bioc/html/DESeq2.html
biomaRt package (v2.44.4)	Durinck et al., 2005 and Durinck et al., 2009	https://bioconductor.org/packages/release/bioc/html/biomaRt.html
ToppGene and ToppCluster	Chen et al. (2009)	https://toppgene.cchmc.org
SynGO	Koopmans et al. (2019)	https://www.syngoportal.org
MaxLive MEA acquisition and analysis software	MaxWell Biosystems	https://www.mxwbio.com/products/maxone-mea-system-microelectrode-array/maxlab-live-software/

RESOURCE AVAILABILITY

Lead contact

Further information and requests for resources and reagents should be directed to and will be fulfilled by the lead contact, ChangHui Pak (cpak@umass.edu).

Materials availability

Engineered hESC lines generated in this study are available upon request.

Data and code availability

- A complete set of bulk RNA sequencing data is publicly available on NCBI Gene Expression Omnibus (GEO) as of 4 April 2022. GSE accession number is GSE199910 and can also be found in the key resources

table. This paper also analyzes existing, publicly available data. This GEO accession number for previously published datasets are listed in the key resources table.

- This paper does not report original code.
- Any additional information required to reanalyze the data reported in this paper is available from the lead contact upon request.

EXPERIMENTAL MODEL AND SUBJECT DETAILS

Cell lines: H1 human embryonic stem cell (ESC) line (male cell line, WiCell) and subsequent engineered ESC lines were cultured under feeder-free conditions as previously described (Pak et al., 2015, 2021). Briefly, ESCs were maintained in mTesR medium and grown on Matrigel (Corning) coated plates. Cells were routinely passaged using ReLeSR (Stem Cell Technologies) every 3–4 days, and upon passaging, Y-27632 (10 uM; Axon Medchem) was added to the media to enhance survival. Cell lines were expanded and banked to create master stock and working stocks. All experiments were limited to ~10 passages in culture from working stocks. Cells were cultured at 37°C with 5% CO_2 and routinely tested for mycoplasma.

CASK knockout lines were generated using CRISPR-mediated gene editing. Briefly, unique sgRNA (5′-CACCGGGACATAGTATTTGAAAGAC-3′) was cloned into lenti-CRISPRv2 construct (Addgene #52961), which expresses Cas9 and puromycin cassette. Lenti-CRISPRv2 plasmid was nucleofected in H1 ESCs using 4D Nucleofector kit (Lonza), and cells were recovered in mTeSR medium. 48 h of puromycin selection allowed propagation of ESCs that successfully carried lenti-CRISPRv2 construct. Cells were replated for single colony picking and expansion. PCR screen was used to confirm CRISPR-mediated genomic deletions. PCR fragments were validated using Sanger sequencing for positive clones. Two independent KO clones were established (KO1 and KO2) which carried 14-bp and 10-bp deletions respectively, which resulted in frameshifts and complete KO. Clones were checked for karyotype and mycoplasma regularly. Neurons were differentiated from working stocks and carried on for no more than ~10 passages.

METHOD DETAILS

Gene targeting

H1 human male embryonic stem cell (ESC) line (WiCell) was cultured under feeder-free conditions. Human ESCs were maintained in mTesR medium and passaged using ReLeSR (Stem Cell Technologies). From this wild-type genetic background, CASK knockout lines were generated using CRISPR-mediated gene editing. Briefly, unique sgRNA (5′-CACCGGGACATAGTATTTGAAAGAC-3′) was cloned into lenti-CRISPRv2 construct (Addgene #52961), which expresses Cas9 and puromycin cassette. Lenti-CRISPRv2 plasmid was nucleofected in H1 ESCs using 4D Nucleofector kit (Lonza), and cells were recovered in mTeSR medium. 48 h of puromycin selection allowed propagation of ESCs that successfully carried lenti-CRISPRv2 construct. Cells were replated for single colony picking and expansion. PCR screen was used to confirm CRISPR-mediated genomic deletions. PCR fragments were validated using Sanger sequencing for positive clones. Two independent KO clones were established (KO1 and KO2) which carried 14-bp and 10-bp deletions respectively, which resulted in frameshifts and complete KO. Clones were checked for karyotype and mycoplasma regularly. Neurons were differentiated from working stocks and carried on for no more than ~10 passages.

Generation of iN cells from human ESCs

On day −1 (d-1), 90–95% confluent ESC cultures were dissociated with Accutase (Innovative Cell Technologies) and plated in 6-well plates at a cell density of 1.0 million cells distributed across 6 wells. Simultaneously, cells along with Ngn2 and rtTA lentiviruses were included in the fresh mTeSR+ medium plus Y-27632 (Axon Medchem) used to plate ESCs. On d0, culture medium was replaced with N2/DMEM-F12/NEAA (Thermo Fisher) containing human BDNF (10 ug/L, Peprotech), human NT-3 (10 ug/L, Peprotech), and mouse laminin (0.2 mg/L, Life Technologies). Doxycycline (2 mg/L, Clontech) was also included on d0 to induce TetO gene expression by binding to rtTA and the TetO promoter upstream of the *Ngn2* gene. Doxycycline was included in all subsequent media changes until d10. To select for Ngn2-iN cells, puromycin (1 mg/L, Invivogen) was added to each media change the following two days. Following selection on d3, Ngn2-iNs were co-cultured with mouse glia and plated in 24-well plates (100,000 iN cells/well; 100,000 glial cells/well). Each well contained a Matrigel (BD Biosciences)-coated glass coverslip, and co-cultures were plated in Neurobasal medium (Thermo Fisher) containing B27 supplement, Glutamax (Life

Technologies), human BDNF, human NT-3, mouse laminin, and Ara-C (2 uM, Sigma) to inhibit glial proliferation. After co-culture, 50% of the medium was replaced every 2–3 days for each well. iN cells that were cultured up to day 7 followed the same media regimen in the absence of mouse glia. On d10, 50% of medium was replaced by MEM-based maturation medium containing MEM supplemented with 0.5% glucose, 0.02% NaHCO3, 0.1 mg/mL transferrin, 5% FBS, 0.5 mM L-glutamine, 2% B27, and 2 μM AraC. On d13, 50% of medium was supplemented with maturation medium, and media change occurred weekly until maturity.

Lentivirus production

Lentiviruses were generated using calcium phosphate transfection of female human embryonic kidney (HEK293T) cells (Chen and Okayama, 1987) in tandem with three lentiviral packaging plasmids: pRSV-REV, pMDLg/pRRE and vesicular stomatitis virus G protein expression vector (VSVG). Per every 75 cm^2 of culture area, 12 ug of lentiviral vector DNA was combined with 3.9 ug REV, 8.1 ug RRE, and 6 ug VSVG helper plasmid DNA. 48 h following the initial transfection, lentiviruses were harvested from each flask, pelleted by centrifugation (90,000 xg for 120 min), resuspended in MEM, aliquoted, and frozen at −80°C.

Primary glia culture

Primary mouse glial cells were collected from the cerebral cortex of the forebrain of newborn wild-type CD1 mice between postnatal days 0–2 (P0-2). Sex of each mouse pup was not determined. Brains were dissected on ice under a light microscope and collected in 1X HBSS (recipe). Mouse cortices were digested using papain (Worthington) and EDTA for 30 min and triturated to dissociate cells. Glia were plated on T75 flasks in DMEM with 10% FBS (Hyclone, GE life sciences) and 5% Pen/Strep (Gibco). Once glia reached confluency, cells were trypsinized and plated at 1/3 density. Glia splitting was repeated an additional two times to guarantee the removal of any remaining mouse neurons. Glia were subsequently used for co-culturing with iN cells.

Sparse transfection in iN cells

To quantify changes in neurite outgrowth, Ngn2-iNs were sparsely transfected with SYN-EGFP construct at either day 4 (for immature iN harvest) or day 14 (for mature iN harvest) using calcium phosphate-based transfection. Briefly, per one well of a 24-well format, 0.5 ug of GFP plasmid, 2.5-M $CaCl_2$, and molecular-grade water was mixed and added dropwise to 2X HBS (280 mM NaCl, 1.5 mM Na_2HPO_4, 50 mM HEPES) on a gentle vortex, and transfection mix incubated at room temperature for 10 min. After washing wells three times with MEM+++ (MEM containing 0.5 mM $CaCl_2$, 1 mM $MgCl_2$, and 4% sucrose to minimize coverslip peeling), transfection mix was added dropwise to each well and incubated for 30 min at 37°C. Wells were washed three final times with MEM+++, and transfection efficiency was confirmed 48 h later.

Immunohistochemistry

Immature d4-transfected iN cell coverslips were harvested on d7, and mature d14-transfected iN cell coverslips were harvested on d28. All coverslips were fixed in 4% paraformaldehyde in PBS+++ (D-PBS containing 0.5 mM $CaCl_2$, 1 mM $MgCl_2$, and 4% sucrose to minimize coverslip peeling) for 20 min at room temperature and washed three times with PBS+++. For immature d4 iN cells, coverslips were mounted to microscope slides using Fluoromount DAPI (Southern Biotech) mounting media. For mature d28 iN cells following fixation, coverslips were incubated in 0.2% Triton X-100 in PBS+++ on a slow belly dancer for 10 min, and cells were blocked in PBS+++ containing 10% goat serum for 1 h at room temperature. Primary antibodies used were: rabbit anti-Synaptophysin (1:2000, Abcam ab14692), mouse anti-PSD-95 (1:1000, Invitrogen MAI-046), chicken anti-MAP2 (1:5000, Abcam ab5392), mouse anti-TAU (1:1000, Invitrogen MN1000) and chicken anti-GFP (1:1000, Aves GFP-1010). Each primary antibody was separately added to a mix of 0.1% triton and 5% goat serum and incubated overnight at 4°C. Coverslips were washed three times with PBS+++, and secondary antibodies (1:400) in 5% goat serum were applied for 1 h. Alexa 546- and Alexa 633-conjugated secondary antibodies (1:1000) were obtained from Invitrogen. Following three final PBS+++ washes, coverslips were mounted to microscope slides with Fluoromount DAPI mounting media.

Bulk RNA sequencing and differential gene expression analysis

Four independent culture replicates of immature d7 and mature d28 iN cells were lysed, and RNA was extracted using the RNeasy kit (Qiagen). RNA-seq libraries were generated from total RNA using NEBNext

Ultra Directional RNA Library Prep Kit for Illumina (NEB). Paired-end sequencing (2 x 75 base-pair reads) was performed using the Illumina Next-seq 500 platform (UMass Amherst Genomics Core), and the resultant fastq files were used for further processing and differential gene expression analysis.

Quantitative RT-PCR

Total RNA was lysed from cells and extracted using RNAeasy kit (Qiagen). Purified RNA was further treated with RNase-free DNase (Qiagen) to remove genomic DNA contamination and eluted in 40–60 μL per sample. Purified total RNA (~40 μg per reaction) was reverse-transcribed and PCR-amplified using Taqman Fast Virus 1-Step Master Mix (Applied Biosystems) and primetime assays for specific genes (IDT). mRNA levels were quantified by real-time PCR assay using the Quantstudio 3 System and RQ analysis software (Thermo Fisher Scientific). qRT-PCR was performed for each of four independent culture replicates for both d7 and d28 neurons. Within each d7 plate, the housekeeping gene *GAPDH* was included as an internal control. Since mouse glia co-cultured with d28 iNs also express *GAPDH*, the neuron-specific *MAP2* gene acted as the internal control for the mature timepoint. Primetime (IDT) sequences for qRT-PCR can be found in the Key resources table.

Immunoblotting

Neurons were washed 3x with DPBS and lysed with RIPA buffer (150 mM NaCl, 5 mM EDTA, 1% Triton X-100, 0.1% SDS, 25 mM Tris-HCl, pH 7.6, and 1x cOmplete protease inhibitor cocktail (Sigma-Aldrich)). Lysates were subjected to SDS-PAGE and immunoblotting using the following primary antibodies: mouse anti-CASK (1:1000; 75–000; Neuromab) and mouse anti-TUJ1/TUBB3 (1:1000; 801201; Biolegend). Fluorescently labeled secondary donkey anti-mouse antibody was used (IRDye 800CW, 1:15,000) and signals were detected with an Odyssey Infrared Imager and Odyssey software (LI-COR Biosciences). Signals were normalized for TUJ1 probed on the same blots as loading controls.

High-density microelectrode array (HD-MEA) network electrophysiology

Network activity and burst recordings were performed using Maxwell Biosystems' CMOS-based single-well MaxOne HD-MEA recording system and accompanying MaxLive software. During each recording, chips were located inside a 37°C, 5% CO_2 incubator. An initial activity scan was performed to identify active electrodes across the array using the full-scan configuration (20-min recording). Once active electrodes were determined, network activity was measured over 10 min from only the electrodes identified as active during the activity scan. To call signals as "events" from the activity scan, the following thresholds were used: 0.10 Hz (firing rate); 20 μV (amplitude); 200 ms (inter-spike interval). The following network activity thresholding parameters for calling action potentials and network bursts were used: 0.3 s (smoothing window size); 1.2 (burst detection threshold), 1 s (minimum peak distance); 0.3 (start-stop threshold). MEA data was exported to Prism (9.3.0) for statistical analysis and graphing.

Preparation of MEA chips

The MaxWell Biosystems CMOS-based single-well MaxOne HD-MEA recording system was used for all network electrophysiology experiments according to the manufacturer's protocols (Maxwell Biosystems, Zurich, Switzerland). Prior to cell plating, MEA chips were sterilized and pre-coated as follows. First, 1 mL of 1% Terg-a-zyme (Alconox) in deionized water was added to each recording array to increase the hydrophilicity of the chip surface. After incubating at room temperature for at least 18 h, the solution was removed, and chips were rinsed with deionized water. MEA chips were sterilized in 70% ethanol for 30 min at room temperature in the biosafety cabinet and washed three times with sterile deionized water. To prepare MEA chips for cell plating, a primary coat of sterile 0.07% poly(ethyleneimine) (PEI) (Sigma/Merck) was applied to each chip and incubated in a 37°C, 5% CO_2 incubator for at least 1 h. A secondary coat of laminin (0.02 mg/mL; Sigma/Merck) was added, and chips incubated at 37°C, 5% CO_2 for at least 1 h to ensure subsequent cell adhesion to the electrode array. 50 μL of d3 co-cultured cells (150,000 iNs:150,000 glia) suspended in B27-supplemented neurobasal medium were plated on top of the electrode array, and chips were left to incubate at 37°C, 5% CO_2 for 1 h to allow cells to adhere to the chips. A supplemental 700 μL of B27 medium was added to each MEA well, and chips incubated overnight at 37°C, 5% CO_2. Media was changed according to the established Ngn2 culture protocol throughout the experiment, with media change days falling one day prior to each recording.

Whole-cell patch-clamp single-cell electrophysiology

All electrophysiological recordings for co-cultured iN cells were performed in the whole-cell configuration at room temperature. Patch pipettes were prepared using a Sutter Instruments Model P-1000 Flaming/Brown micropipette puller and borosilicate glass capillary tubes (Sutter Instruments). Intracellular (internal) solution was added to each patch pipette using a microfil needle (World Precision Instruments), and pipette resistance ranged between 3.9 and 14.7 MOhm. A K-gluconate-based internal pipette solution was used in all experiments, containing (in mM): 126 K-gluconate, 4 KCl, 10 HEPES pH 7.2, 4 Mg-ATP, 0.3 Na_2-GTP and 10 phosphocreatine; 270–290 mOsm/l; pH 7.2, adjusted with KOH after each reagent addition. The bath solution in all experiments contained (in mM): 130 NaCl, 5 KCl, 2 $CaCl_2$, 1 $MgCl_2$, 10 HEPES, 10 glucose; 290–300 mOsm/L, adjusted with sucrose; pH 7.4, adjusted with NaOH. Data were digitized at 10 kHz with a 2-kHz low-pass filter using a Multiclamp 700A amplifier (Molecular Devices), and cellular intrinsic properties of iN cells, including capacitance and input resistance, were recorded in voltage-clamp mode with a minimal amount of current introduced to hold membrane potentials around −70 mV (typically 5–30 pA). Spontaneous excitatory postsynaptic currents (sEPSCs) were observed for iN cells in voltage-clamp mode with a holding potential of −70 mV and analyzed in Easy Electrophysiology (2.3.3) using the template matching search function and a minimum threshold of 10-pA change in current to call a synaptic event. Action potential parameters, including V_{rest}, and spontaneous APs were recorded after break-in but prior to any current injection. To elicit action potentials, a series of increasing amounts of current was applied to the cell in 5-pA increments across 19 independent sweeps (−50 pA to +130 pA). Each step lasted for 1 s, and action potential kinetics were analyzed in ClampFit (9.02) for the first triggered AP observed at the lowest state of current injection.

QUANTIFICATION AND STATISTICAL ANALYSIS

Whole-cell patch-clamp single-cell electrophysiology analysis

The experimenter was blind to the genotype of all cultures during electrophysiological recordings and analysis, and genotypes were unblinded after analysis was complete. Data wrangling was performed in Microsoft Excel, and all raw data points were transferred to Prism (9.3.0) for basic statistics, outlier detection, significance tests, and graph generation. To identify outliers from pooled replicates, the ROUT outlier test was used to identify outliers by fitting data with nonlinear regression and using a false discovery rate of Q = 1%. An unpaired parametric two-tailed Student's *t* test was performed to compare the two genotypes (WT vs. KO1 or WT vs. KO2) for statistical significance. An unpaired nonparametric Kolmogorov-Smirnov test was performed to determine significant differences between the cumulative probability distributions of sEPSC inter-event intervals and amplitudes. Significance was represented by corresponding asterisks: *$p < 0.05$, **$p < 0.01$, ***$p < 0.001$; nonsignificant comparisons were not indicated.

Image acquisition and quantification of neurite outgrowth and synaptic puncta

All images were taken with a Nikon A1R25 resonant scanning confocal microscope. Neurite outgrowth was captured using a Zeiss Plan-Apochromat 20×/1.40na Oil DIC Objective M27 with 20X magnification at 1024×1024 pixel resolution (aspect ratio: 0.099233 μm per pixel). Synapse formation was imaged using a Zeiss Plan-Apochromat 60×/1.40na Oil DIC Objective M27, and a 2X zoom at 1024x1024 pixel resolution (aspect ratio: 0.099233 μm per pixel). Imaris software (Bitplane), specifically the filamenting and surfaces modules, was used to quantify changes in neurite outgrowth (metrics: number of primary processes, number of branch points, total neurite length, soma size), synapse formation, and synapse size. The following analysis parameters were used: Surface Detail: 0.3 um; Background Subtraction: 1.00 um; Seed Point Diameter: 0.3 um. Filter → Number of Voxels: >10. Dendrite-to-puncta filter → Shortest Distance to Surfaces. Surfaces Dendrite: 0.1 um. Dendrites as close to 150 um in length were chosen to calculate puncta density (but dendritic length ranged greatly). Puncta surface parameters were kept the same for all images. All image quantifications were conducted blindly. Statistical analysis was performed using Student's *t* test comparing WT to each individual KO (*$p < 0.05$, **$p < 0.01$, ***$p < 0.001$; nonsignificant comparisons were not indicated).

Bulk RNA-sequencing and differential gene expression analysis

Bulk RNA-sequencing & differential gene expression analysis (d7)

Raw sequencing reads were processed using an in-house RNA-Seq data processing software Dolphin (Yukselen et al., 2020) at University of Massachusetts Medical School. Paired-end reads fastq files generated from the NextSeq 500 was imported in the Dolphin analysis suite. The fastq files were subjected to quality check using FastQC. The high-quality read-pairs first were filtered out using ribosomal RNAs with bowtie2.

STAR (2.6.0c) alignment tool (Dobin et al., 2013) was used to align the reads to the reference transcriptome. RSEM (v1.2.28) (Li and Dewey, 2011) was used to quantify the expression levels of genes. The reference transcriptome refSeq annotation, UCSC hg19 refGene was used. For DEG analysis, top-ranking genes between control and knockout genotypes were filtered for log2(TPM+1) $\geq$ 1, and a Student's *t* test (two-tailed unequal variance) was performed. DEGs with a cutoff of p value < 0.05 and |log2FC |> 1 were chosen for downstream analysis. K-means clustering and visualization were done in Morpheus. qRT-PCR data represents means $\pm$ SEM, and statistical analysis was performed using Student's *t* test comparing WT to each individual KO (*p < 0.05, **p < 0.01, ***p < 0.001; nonsignificant comparisons were not indicated).

Bulk RNA-sequencing (d28)

On average, 34 million reads per sample were collected using the Illumina Next-seq 500 platform (UMass Amherst Genomics Core). To process paired-end reads, we first built a human + mouse reference (Homo_sapiens GRCh38 v96 and Mus_musculus GRCm38 v96) with a concatenated human-mouse index using the index command in Kallisto (v 0.46.0). d28 RNA-sequencing reads from Fastq files were pseudo-aligned to the concatenated reference genome using the Kallisto quant command, and transcripts were assigned to proper species reference. For each Kallisto-processed human-mouse sample, expression matrices of raw count values and TPM (transcripts per million) were constructed for human-specific transcripts.

Differential gene expression analysis (d28)

Prior to DEG analysis, we first built a transcript-gene conversion table using genecode gene annotation (v39) gtf file (https://ftp.ebi.ac.uk/pub/databases/gencode/Gencode_human/release_39/gencode.v39.annotation.gtf.gz). Transcripts were then loaded and transferred to ensembl gene ids using tximport package (v1.16.1). DESeq2 (v1.28.1) was used to perform DEG analysis for raw count values of 12 d28 samples with the design formula as "design = ~ cell_lines + genotypes", where "cell_lines" is the key of paired samples and "genotypes" is the key of genotype annotations. Significance test results from DESeq2, including log2 fold changes and FDR adjusted p values were used for downstream analysis. Ensembl ids were transferred to gene symbols using biomaRt package (v2.44.4) with Ensembl as the host. For d28 DEG analysis, paired analysis was done in using the generalized linear model in DESeq2, and p values were generated using Wald test. FDR adjusted p values were generated for multiple comparisons.

To generate a list of overlapping DEGs between our d28 transcriptome and transcriptome reported by Becker et al. (2020), we compared our D28 DEGs and DEGs in Table S3 of Becker et al. (2020) study. We used our 3 DEG lists (KO1 vs. WT; KO2 vs. WT; KO1+KO2 vs. WT) and investigated overlapping genes (up/down/both) separately. Genes with adjusted p values <0.05 and absolute log2FC > 0.5 were called DEGs.

Gene set enrichment analysis (GSEA) for both d7 and d28

ToppCluster (Chen et al., 2009), a multiple gene list feature enrichment analyzer, was used for both d7 and d28 DEG datasets to identify significantly enriched or depleted classes of genes, gene families, or biological pathways affected by CASK-KO. Briefly, the differentially expressed gene dataset was input to the ToppCluster software. A 0.05 p-value cutoff using the Bonferroni test was applied to isolate significantly affected gene ontology features, and .xgmml cluster network files were generated and imported into Cytoscape (v3.9.1), an open-source software package for integrating and visualizing these complex molecular interaction and biological pathway networks into string-cluster network maps (Shannon et al., 2003). The enrichment of synaptic genes was analyzed using the SynGO database (Koopmans et al., 2019).

CASK PPI network enrichment analysis for both d7 and d28

ToppCluster (Chen et al., 2009) was used for both d7 and d28 DEG datasets to analyze and generate protein-protein interaction (PPI) networks for known CASK interactors. Briefly, the DEG lists were submitted to the ToppCluster software, and the "Interaction Network" option was selected for analysis. Cytoscape-compatible PPI networks were generated and exported for visualizing primary (direct) and secondary (indirect) protein interactors with CASK (Shannon et al., 2003).